# The Volcanic History and Magmatic Sulfide Mineralogy of Latites of the Central East Tintic Mountains, Utah

Jeffrey D. Keith, R. David Dallmeyer and Choon-Sik Kim[1], Bart J. Kowallis[2]

*Department of Geology, The University of Georgia, Athens, Georgia 30602[1]*

*Department of Geology, Brigham Young University, Provo, Utah 84602[2]*

## Abstract

This report documents several new findings concerning the volcanic history and magmatic sulfide content of latites in the central East Tintic Mountains, Utah. For example, fission-track ages and $^{40}Ar/^{39}Ar$ ages reported here suggest that some of the volcanism and alteration in this area is as old as 37.4 to 35.3 Ma. This early episode of volcanism was contemporaneous with lacustrine deposition; the overlying volcanic rocks and cross-cutting intrusions range in age from about 34.5 to 33.6 Ma. Previous workers had inferred that a large caldera related to the eruption of the younger Packard Quartz Latite (ca. 32-33 Ma) and Fernow Quartz Latite is present beneath these 34.5 to 33.6 Ma volcanic rocks in this area. Consequently, the new ages reported in this paper indicate that either the previously determined age of the Packard Quartz Latite is incorrect or the inferred caldera (related to eruption of the Packard Quartz Latite) is not present. However, data suggest that a smaller caldera related to the eruption of the tuff member of the Copperopolis Latite may be present. It is noted that many monzonite dikes and intrusions in this area are hornblende bearing and are correlative in modal and chemical composition with the productive Silver City Stock rather than the barren Sunrise Peak Stock. The large areas of hydrothermal alteration which surround these intrusions exhibit many similarities to the well-studied alteration halos in the East Tintic District. The age, composition, and field relationships of the post-lacustrine volcanic rocks suggest that they may represent, in part, the extrusive equivalents of the monzonite dikes and Silver City Stock. Data presented here suggest that the Silver City Stock and related intrusions may be part of one of the youngest ($33.6 \pm 0.2$ Ma) igneous events in the central East Tintic Mountains, but not as young as previously suggested (ca. 31.5 Ma).

This paper documents, for the first time, the existence of unusually large (and abundant) magmatic sulfides in lava vitrophyres and vent-facies biotite latite dikes, which are the surface expressions of the Silver City Quartz Monzonite intrusions in this area. In addition, preliminary analytical data suggest that the sulfides host most of the Cu and Ag present in the latites. Magmatic sulfides are preserved only in the least oxidized and least degassed lavas and vitrophyres. Sulfide petrography of other dikes and flows reveals a progressive suite of degassed sulfide compositions and textures which document the removal of Cu and S (and Ag?) from the sulfide bleb. It is proposed that similar degassing processess in sub-volcanic intrusions may have made substantial contributions to an ore fluid. The East Tintic Mountains are potentially the first locality, worldwide, where Cu and Ag in mesothermal veins can be demonstrated to be derived from degassed Cu-Ag-bearing magmatic sulfides. Consequently, the central East Tintic Mountains are a favorable area for exploration for Ag (Pb-Zn-Cu-Au) ore bodies because: 1) productive monzonite intrusions are present, and 2) Paleozoic rocks favorable for ore deposition may be present beneath relatively thin volcanic cover because the area is not entirely enclosed within a caldera.

## Introduction

Morris and Lovering (1979) suggest that the ages of all the volcanic and intrusive units in the East Tintic Mountains cluster into two groups of about 32 to 33 Ma and 18 Ma. However, they do report some older ages (35 to 39 Ma), which they consider to be anomalous. They suggest that most volcanic units in the East Tintic District were deposited in an area of moderate topographic relief, analogous to the East Tintic Mountains today. They hypothesize that the initial ash-flow eruption deposited the Packard Quartz Latite and Fernow Quartz Latite and created a caldera 14 km in diameter in the central portion of the East Tintic Mountains (Figure 1; Morris, 1975). Subsequently, latite flows, ash flows, and hypabyssal intrusions of the Tintic Mountain Volcanic Group filled and overflowed the caldera. These two events were followed closely in time by a final episode of Oligocene latitic volcanism and consanguineous intrusions (Silver City stock and correlative dikes; Figure 1) which appears to be genetically related to all of the mineralization in these districts (Morris and Lovering, 1979).

This report documents the occurrence of previously unrecognized Eocene-Oligocene (ca. 37 to 35 Ma) volcanic and intrusive rocks and lacustrine sedimentary rocks (up to 50 m thick). These events were followed by volcanic and intrusive activity which ranged in age from

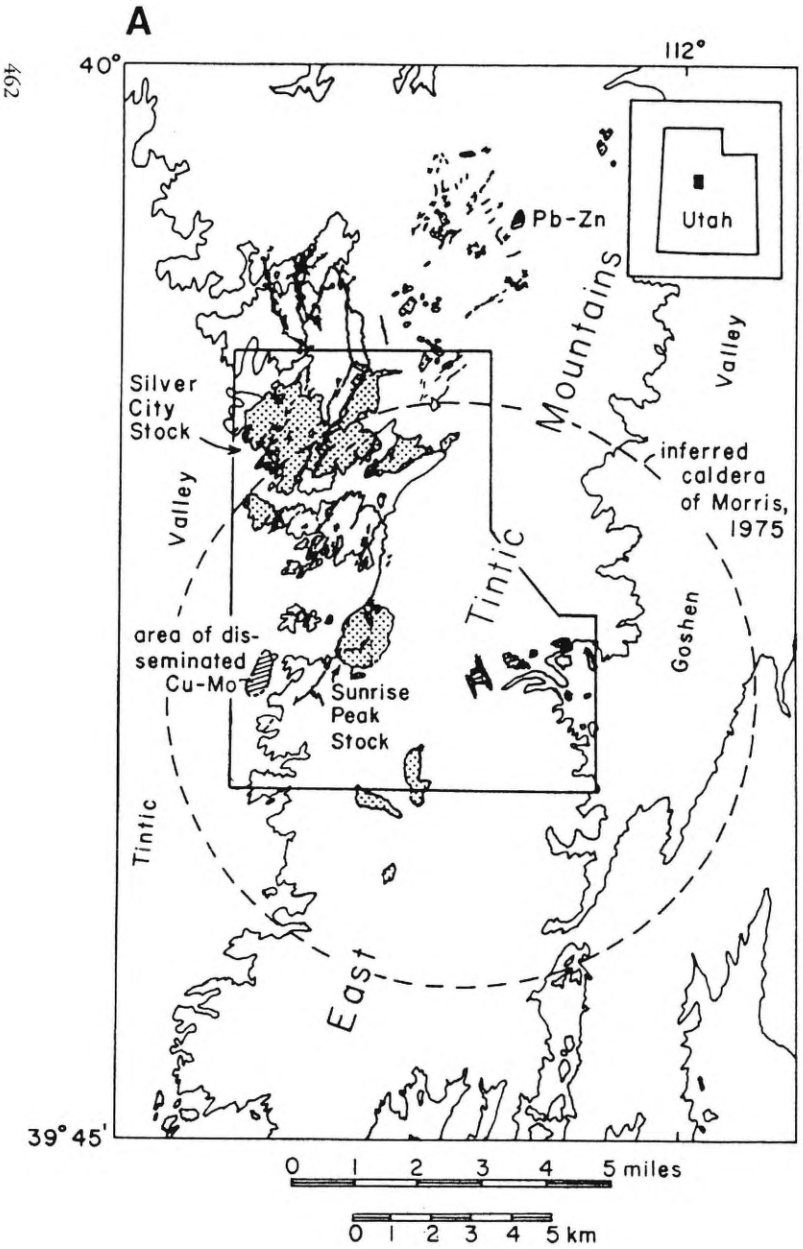
A
40°
112°
Utah
Pb-Zn
Silver City Stock
Valley
Tintic Mountains
Valley
inferred caldera of Morris, 1975
area of disseminated Cu-Mo
Sunrise Peak Stock
Tintic
Goshen
East
39° 45'
0 1 2 3 4 5 miles
0 1 2 3 4 5 km

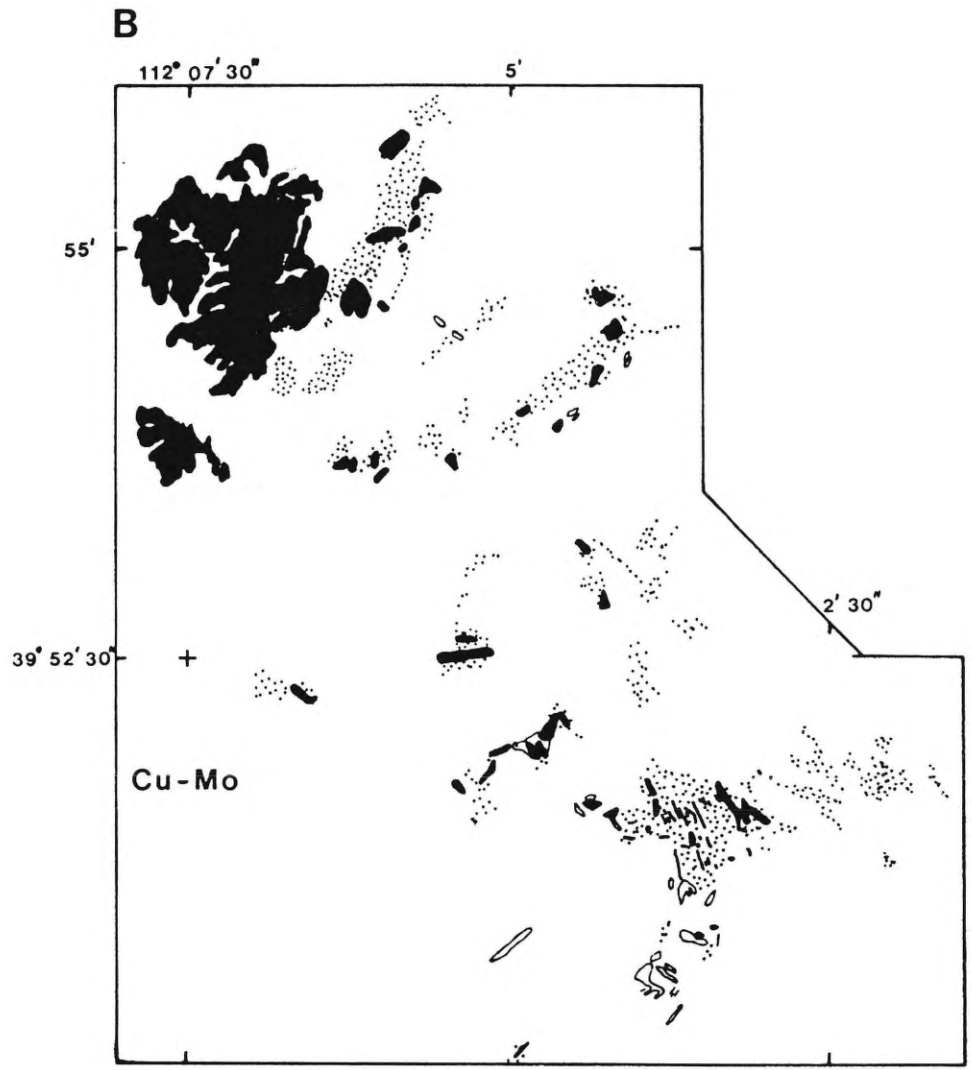
B
112° 07' 30"
5'
55'
2' 30"
39° 52' 30"
Cu-Mo

Figure 1. A. Ore deposits, monzonite stocks, inferred caldera of Morris (1975), and index map of the East Tintic Mountains (compiled from Morris, 1975; Morris and Morgensen, 1978). Replacement and vein ore deposits are shown as solid black; monzonite intrusions are stippled (sills of Morris (1975) are not shown); other features as labeled in figure. Part of the area mapped by Keith and Kim during the summer of 1988 is outlined and summarized in part B. The immediate vicinity of the sub-economic Cu-Mo deposit is covered by alluvium or unmapped (mapped by Hannah and Macbeth, 1990). B. Map summarizing the relationship between monzonite intrusions of Silver City lithology (in solid black), argillic-phyllic alteration and moderate to intensely silicified rock (stippled). In addition, biotite latite dikes (outlined only), some of which contain magmatic sulfides are also summarized from Keith et al. (1989b).

roughly 34.5 to 33.6 Ma. The study area also includes an area of strong hydrothermal alteration and diking in the central East Tintic Mountains (Figure 1). The alteration assemblages present in this area (silicification and abundant pyrite in carbonate-bearing sedimentary rocks) suggest several analogies to alteration in the East Tintic District.

The lacustrine sedimentary rocks clearly affected the character of the widespread hydrothermal alteration in Government Canyon. Alteration products in the volcanic rocks overlying the sedimentary rocks are indicative of more neutral pH conditions compared to the argillic alteration below the sedimentary rocks. In addition, larger amounts of pyrite and jasperoid are generally found in the sediments than in subjacent volcanic rocks. These and other facets of the alteration assemblages present in Government Canyon are very analogous (and probably of equivalent age) to the well-studied alteration halos in volcanic rocks in the East Tintic District (Lovering, 1949). At the surface, acidic hydrothermal solutions in Government Canyon were mostly neutralized during passage through Oligocene sediments rather than along veins in Paleozoic rocks. However, several lines of reasoning suggest that the volcanic cover becomes thinner to the east and north in this portion of the East Tintic Mountains; consequently, exploration in areas of favorable hydrothermal alteration and potentially thin volcanic cover may be practical.

The Tintic and East Tintic Districts have long been recognized as clearly exemplifying the spatial relationships between sulfide-rich alteration, Ag (-Au) mineralization, and productive intrusions (Lindgren and Loughlin, 1919; Lovering, 1949; Morris and Lovering, 1979). However, whether the precious metals are derived from the intrusions or merely leached from the country rock by hydrothermal circulation has not been convincingly demonstrated for this district or any epithermal-mesothermal vein deposit. Our recent work has documented the existence of unusually large *magmatic* sulfides in vent-facies dikes (and lava vitrophyres) which are the surface expressions of the productive intrusions in the East Tintic Mountains(Keith et al., 1989a). In addition, preliminary analytical data suggest that the sulfides may host most (~75%) of the Ag present in the latites. Such a close correspondence between intrusions with unusually abundant magmatic sulfides and hydrothermal mineralization has not been previously demonstrated. However, Whitney and Stormer (1983) speculated that a general relationship between degassing calc-alkaline pyrrhotite-bearing magmas and hydrothermal ore deposits was possible. The East Tintic Mountains are potentially the first locality, worldwide, where Ag in mesothermal veins can be demonstrated to be derived from degassed Ag-bearing magmatic sulfides.

## Methods

### X-Ray Fluorescence and Electron Microprobe Techniques

Approximately 150 samples of extrusive and intrusive units were collected and examined in thin section or polished section. Whole-rock sulfur analyses were done by X-ray fluorescence spectrometry using pressed powder pellets with G-2, GSP-1, and W-1 as standards. Whole-rock major elements were analysed using a fused disk procedure (Norish and Hutton, 1969) with the USGS standard AGV-1 used as an internal standard. Microprobe analyses were done at the University of South Carolina using a Cameca SX-50 electron microprobe. Descriptions and locations of samples used for analysis are given in Keith et al. (1989b). An appendix of sample petrography and sample locations is available from the first author on request.

### $^{40}Ar/^{39}Ar$ Analytical Techniques

Optically pure (> 99%) mineral concentrates were wrapped in aluminum-foil packets, encapsulated in sealed quartz vials and irradiated in either the U.S. Geological Survey TRIGA reactor (samples HS-UTH-86-2, TJ-84-88, TJ-112-88, TJ-77-88) or the H-5 position of the Ford Reactor at the University of Michigan (samples TJ-8-87 and KS-2A-87). Variations in the flux of neutrons along the length of the irradiation assembly were monitored with several mineral standards, including MMhb-1 (Alexander et al. 1978). The samples were incrementally heated until fusion in a double-vacuum, resistance heated furnace. Temperatures were monitored with a direct-contact thermocouple and are controlled to $\pm$ 1°C between increments and are accurate to $\pm$ 5°C. Measured isotopic ratios were corrected for total system blanks and the effects of mass discrimination. Interfering isotopes produced during irradiation were corrected using factors reported by Dalrymple et al. (1981) for the TRIGA reactor or Harrison and Fitzgerald (1986) for the Ford Reactor. Apparent $^{40}Ar/^{39}Ar$ ages were calculated from the corrected isotopic ratios using the decay constants and isotopic abundance ratios listed by Steiger and Jager (1977).

Two categories of uncertainties are encountered in $^{40}Ar/^{39}Ar$ incremental-release dating. One group involves intralaboratory uncertainties related to measurement of the isotopic ratios used in the age equation. The other group considers interlaboratory uncertainties in other parameters used in the age equation (monitor age, J-value determination, etc.), and are the same for each gas increment evolved from a particular sample. Therefore, to evaluate the significance of incremental age variations within a single sample, only intralaboratory uncertainties should be considered. These are reported here and have been calculated by statistical propagation of uncertainties associated with measurement of each isotopic ratio (at two standard deviations of the mean) through the age equation. Interlaboratory uncertainties are approximately 1.25-1.50% of the quoted age. Total-gas ages have been computed for each sample by appropriate weighting of the age and percent $^{39}Ar$ released within each temperature increment. A "plateau" is herein considered to be defined if the ages recorded by two or more contiguous gas fractions, each representing >4% of the total $^{39}Ar$ evolved and characterized by generally similar apparent K/Ca ratios (and together constituting >50% of the total quantity of $^{39}Ar$ evolved) are mutually similar within a $\pm$ 1% intralaboratory uncertainty. Analyses of the MMhb-1 monitor indicate that apparent K/Ca ratios may be calculated through the relationship 0.518 ( $\pm$ 0.005) x $^{39}Ar/^{37}Ar$ corrected (TRIGA reactor) or 0.505 ( $\pm$ 0.003) x $^{39}Ar/^{37}Ar$ corrected (Ford Reactor).

Plateau portions of the analyses have been plotted on $^{36}Ar/^{40}Ar$ vs. $^{39}Ar/^{40}Ar$ isotope correlation diagrams. Regression techniques followed the methods of York (1969). A mean square of the weighted deviates (MSWD) is the statistical parameter which has been used to evaluate isotopic correlations. Roddick (1978) suggests that an MSWD > c. 2.5 indicates scatter about a correlation line greater than that which can be explained only by experimental errors.

## Results

### $^{40}Ar/^{39}Ar$ Results

Four biotite, one sanidine, and one muscovite concentrate have been prepared from samples collected within volcanic units exposed in the East Titnic Mountains, Utah. Location coordinates and detailed petrographic descriptions of the analyzed samples are itemized in Keith et al. (1989b). The $^{40}Ar/^{39}Ar$ analytical data are listed in Table 1, and are presented as incremental age spectra in Figure 2. Results of $^{36}Ar/^{40}Ar$ vs. $^{39}Ar/^{40}Ar$ isotope correlations of the analysis are listed in Table 2.

The four biotite concentrates display internally discordant $^{40}Ar/^{39}Ar$ age spectra corresponding to total-gas ages ranging between 37.9 $\pm$ 0.2 Ma (TJ-8-87) and 34.0 $\pm$ 0.4 Ma (HS-UTH-86-2). Apparent K-Ca spectra are internally variable. The low-temperature increments are generally characterized by systematically increasing apparent K/Ca ratios and systematically decreasing apparent ages. Intermediate-temperature gas fractions are characterized by very large and only slightly fluctuating apparent K/Ca ratios. These increments generally record mutually similar apparent ages within each analysis, and define plateau ages of 37.4 $\pm$ 0.3 Ma (TJ-8-87), 35.3 $\pm$ 0.1 Ma (TJ-112-88), 34.5 $\pm$ 0.2 Ma (TJ-84-88), and 33.6 $\pm$ 0.2 Ma (HS-UTH-86-2). Higher temperature portions of each analysis generally display systematically decreasing apparent K/Ca ratios and record somewhat variable apparent ages. The plateau analytical data yield well-defined $^{36}Ar/^{40}Ar$ vs. $^{39}Ar/^{40}Ar$ isotope correlations (MSWD = 0.14-1.84, Table 2) with inverse ordinate intercepts similar to the $^{40}Ar/^{36}Ar$ ratio within the present-day atmosphere (295.5). This indicates a lack of significant extraneous ("excess") argon contamination within constituent biotite grains. Using the inverse abscissa intercepts in the age equation yields plateau isotope correlation ages similar to those calculated for each sample directly from the analytical data.

The muscovite concentrate from sample KS-2A-87 displays internally discordant apparent age and K/Ca spectra with a total-gas age of 36.5 $\pm$ 0.6 Ma. The 450-660°C temperature fractions are characterized by large and generally similar apparent K/Ca ratios. These increments define a plateau age of 36.7 $\pm$ 0.5 Ma. The four high-temperature gas fractions display markedly fluctuating apparent K/Ca ratios and record somewhat variable apparent ages. The plateau data yield an isotope correlation (MSWD = 0.19) with an inverse ordinate intercept of 346.3 $\pm$ 31.3. Using the inverse abscissa intercept in the age equation results in a plateau isotope correlation age of 36.6 $\pm$ 0.2 Ma.

The sanidine muscovite concentrate from sample TJ-77-98 also displays internally discordant apparent age and apparent K/Ca spectra with a total-gas age of 34.3 $\pm$ 0.2 Ma. Apparent K/Ca ratios systematically increase throughout the 700-1020°C portions of the analysis. However, the 800-1020°C increments record mutually similar apparent ages which define a plateau age of 34.1 $\pm$ 0.1 Ma. The two high-temperature increments record lower apparent K/Ca ratios and define younger apparent ages. The plateau analytical data result in an isotope correlation (MSWD = 0.43) with an inverse ordinate intercept of 360.3 $\pm$ 42.6. Using the inverse abscissa intercept in the age equation yields a plateau isotope correlation age of 34.0 $\pm$ 0.1 Ma.

### Interpretation

During the biotite analyses, intrasample fluctuations in apparent K/Ca ratios suggest experimental evolution of argon occurred from several compositionally distinct, and variably retentive phases. These could be represented by: 1) very minor, optically undetectable mineralogical contaminants in the biotite concentrates; 2) petro-

# Table 1

## $^{40}AR/^{39}AR$ Analytical Data for Incremental Heating Experiments on Minerals From Volcanic Units in the East Tintic Mountains, Utah.

| Release temp (°C) | $(^{40}Ar/^{39}Ar)$* | $(^{36}Ar/^{39}Ar)$* | $(^{37}Ar/^{39}Ar)^c$ | $^{39}Ar$ % of total | $\%^{40}Ar$ non-atmos.* | $^{36}Ar_{Ca}$ % | Apparent Age (Ma)** |
|---|---|---|---|---|---|---|---|
| **Biotite** | | | | | | | |
| Sample TJ-8-87: J = 0.00631 | | | | | | | |
| 475 | 7.75 | 0.02444 | 0.021 | 0.48 | 6.32 | 0.02 | 5.6 ± 9.3 |
| 610 | 18.09 | 0.04679 | 0.149 | 0.27 | 23.44 | 0.09 | 47.7 ± 16.1 |
| 645 | 8.76 | 0.01818 | 0.079 | 0.76 | 38.36 | 0.12 | 37.9 ± 4.2 |
| 680 | 5.62 | 0.00721 | 0.014 | 1.94 | 61.41 | 0.06 | 38.9 ± 1.6 |
| 715 | 4.09 | 0.00252 | 0.007 | 6.53 | 80.87 | 0.08 | 37.2 ± 0.7 |
| 750 | 3.64 | 0.00140 | 0.005 | 13.03 | 87.58 | 0.10 | 36.0 ± 0.2 |
| 775 | 3.64 | 0.00087 | 0.006 | 11.68 | 91.89 | 0.19 | 37.7 ± 0.3 |
| 800 | 3.59 | 0.00103 | 0.005 | 13.41 | 90.48 | 0.14 | 36.7 ± 0.2 |
| 825 | 3.61 | 0.00074 | 0.003 | 17.70 | 92.92 | 0.11 | 37.8 ± 0.3 |
| 850 | 3.70 | 0.00084 | 0.004 | 18.93 | 92.23 | 0.15 | 38.4 ± 0.3 |
| Fusion | 4.03 | 0.00105 | 0.011 | 15.27 | 91.40 | 0.29 | 41.5 ± 0.4 |
| Total | 3.86 | 0.00156 | 0.007 | 100.00 | 89.00 | 0.16 | 37.9 ± 0.4 |
| Total without 475-680°C and fusion | | | | 81.28 | | | 37.4 ± 0.3 |
| **Sample TJ-112-88: J = 0.009245** | | | | | | | |
| 500 | 9.82 | 0.01669 | 0.283 | 0.74 | 49.95 | 0.46 | 80.0 ± 1.6 |
| 600 | 6.63 | 0.00703 | 0.132 | 1.27 | 68.72 | 0.51 | 74.4 ± 1.6 |
| 650 | 4.38 | 0.00448 | 0.039 | 2.04 | 69.69 | 0.24 | 50.2 ± 0.9 |
| 690 | 2.95 | 0.00209 | 0.017 | 7.11 | 78.92 | 0.22 | 38.4 ± 0.4 |
| 725 | 2.37 | 0.00065 | 0.013 | 10.18 | 91.65 | 0.54 | 35.9 ± 0.1 |
| 750 | 2.22 | 0.00035 | 0.009 | 11.30 | 95.07 | 0.69 | 34.9 ± 0.2 |
| 775 | 2.19 | 0.00028 | 0.008 | 11.03 | 95.95 | 0.73 | 34.7 ± 0.1 |
| 800 | 2.20 | 0.00026 | 0.008 | 9.95 | 96.27 | 0.83 | 35.0 ± 0.2 |
| 825 | 2.29 | 0.00044 | 0.012 | 6.34 | 94.14 | 0.76 | 35.7 ± 0.2 |
| 960 | 2.46 | 0.00099 | 0.014 | 17.51 | 87.94 | 0.39 | 35.8 ± 0.1 |
| Fusion | 2.44 | 0.00105 | 0.030 | 22.54 | 87.13 | 0.78 | 35.2 ± 0.1 |
| Total | 2.54 | 0.00105 | 0.020 | 100.00 | 89.51 | 0.62 | 36.6 ± 0.2 |
| Total without 500-690°C | | | | 88.84 | | | 35.3 ± 0.1 |
| **Sample TJ-84-88: J = 0.009622** | | | | | | | |
| 525 | 15.64 | 0.04150 | 0.369 | 0.62 | 21.76 | 0.24 | 58.1 ± 5.3 |
| 625 | 3.23 | 0.00433 | 0.084 | 1.27 | 60.36 | 0.53 | 33.5 ± 0.7 |
| 675 | 2.45 | 0.00140 | 0.047 | 2.25 | 83.09 | 0.91 | 35.0 ± 0.5 |
| 710 | 2.19 | 0.00056 | 0.021 | 5.75 | 92.20 | 1.02 | 34.6 ± 0.3 |
| 740 | 2.08 | 0.00031 | 0.010 | 9.32 | 95.34 | 0.89 | 34.1 ± 0.2 |
| 765 | 2.06 | 0.00021 | 0.007 | 10.43 | 96.66 | 0.90 | 34.2 ± 0.1 |
| 790 | 2.08 | 0.00029 | 0.007 | 10.62 | 95.60 | 0.62 | 34.1 ± 0.2 |
| 813 | 2.11 | 0.00044 | 0.007 | 9.88 | 93.52 | 0.41 | 33.9 ± 0.2 |
| 840 | 2.16 | 0.00055 | 0.007 | 8.95 | 92.27 | 0.33 | 34.3 ± 0.2 |
| 870 | 2.30 | 0.00096 | 0.008 | 10.24 | 87.47 | 0.22 | 34.6 ± 0.1 |
| 905 | 2.56 | 0.00176 | 0.010 | 8.26 | 79.50 | 0.16 | 35.0 ± 0.4 |
| 940 | 2.92 | 0.00291 | 0.017 | 6.75 | 70.39 | 0.16 | 35.3 ± 0.7 |
| 980 | 2.92 | 0.00291 | 0.023 | 8.67 | 70.37 | 0.22 | 35.3 ± 0.4 |
| 1020 | 2.79 | 0.00255 | 0.057 | 6.13 | 72.93 | 0.61 | 35.0 ± 0.5 |
| Fusion | 2.47 | 0.00245 | 0.478 | 0.87 | 71.92 | 5.30 | 30.5 ± 2.3 |
| Total | 2.44 | 0.00142 | 0.022 | 100.00 | 86.15 | 0.55 | 34.6 ± 0.4 |
| Total without 525-625°C and fusion | | | | 97.24 | | | 34.5 ± 0.2 |

## Table 1 (Continued)

| Release temp (°C) | $(^{40}Ar/^{39}Ar)^*$ | $(^{36}Ar/^{39}Ar)^*$ | $(^{37}Ar/^{39}Ar)^c$ | $^{39}Ar$ % of total | $\%^{40}Ar$ non-atmos.$^+$ | $^{36}Ar_{Ca}$ % | Apparent Age (Ma)** |
|---|---|---|---|---|---|---|---|
| **Sample HS-UTH-86-2: J = 0.009895** | | | | | | | |
| 525 | 10.37 | 0.02782 | 0.104 | 2.47 | 20.72 | 0.10 | 37.9 ± 2.4 |
| 625 | 6.00 | 0.01315 | 0.028 | 7.75 | 35.23 | 0.06 | 37.4 ± 0.9 |
| 675 | 2.52 | 0.00202 | 0.012 | 11.44 | 76.07 | 0.16 | 33.9 ± 0.2 |
| 710 | 2.18 | 0.00090 | 0.010 | 11.30 | 87.53 | 0.30 | 33.7 ± 0.1 |
| 735 | 2.15 | 0.00077 | 0.012 | 7.11 | 89.20 | 0.42 | 33.9 ± 0.2 |
| 760 | 2.16 | 0.00098 | 0.012 | 5.38 | 86.37 | 0.33 | 33.1 ± 0.3 |
| 785 | 2.26 | 0.00115 | 0.012 | 4.68 | 84.71 | 0.29 | 33.8 ± 0.4 |
| 810 | 2.47 | 0.00181 | 0.019 | 3.87 | 78.08 | 0.28 | 34.0 ± 0.3 |
| 840 | 2.48 | 0.00179 | 0.022 | 4.69 | 78.52 | 0.33 | 34.4 ± 0.6 |
| 875 | 2.38 | 0.00144 | 0.022 | 5.90 | 82.00 | 0.42 | 34.6 ± 0.5 |
| 910 | 2.26 | 0.00124 | 0.021 | 8.81 | 83.53 | 0.45 | 33.4 ± 0.2 |
| 945 | 2.13 | 0.00083 | 0.019 | 14.69 | 88.22 | 0.62 | 33.2 ± 0.2 |
| Fusion | 2.09 | 0.00074 | 0.039 | 11.90 | 89.49 | 1.45 | 33.2 ± 0.3 |
| Total | 2.74 | 0.00276 | 0.022 | 100.00 | 79.30 | 0.48 | 34.0 ± 0.4 |
| Total without 525, 625, 945°C and fusion | | | | 89.78 | | | 33.6 ± 0.2 |
| **Muscovite** | | | | | | | |
| **Sample KS-2A-87: J = 0.006345** | | | | | | | |
| 450 | 4.25 | 0.00291 | 0.013 | 11.72 | 78.89 | 0.13 | 38.0 ± 0.4 |
| 475 | 3.57 | 0.00094 | 0.012 | 14.30 | 91.19 | 0.38 | 36.9 ± 0.5 |
| 500 | 3.70 | 0.00136 | 0.013 | 12.27 | 88.13 | 0.41 | 37.0 ± 0.3 |
| 525 | 3.49 | 0.00066 | 0.012 | 16.86 | 93.37 | 0.54 | 36.9 ± 0.5 |
| 550 | 3.47 | 0.00070 | 0.012 | 15.99 | 92.99 | 0.50 | 36.6 ± 0.3 |
| 575 | 3.52 | 0.00085 | 0.011 | 5.70 | 91.82 | 0.50 | 36.6 ± 0.5 |
| 600 | 3.45 | 0.00099 | 0.010 | 6.31 | 90.48 | 0.30 | 35.4 ± 1.2 |
| 625 | 3.71 | 0.00202 | 0.010 | 5.72 | 82.89 | 0.14 | 34.8 ± 0.5 |
| 660 | 3.72 | 0.00175 | 0.017 | 3.68 | 85.08 | 0.27 | 35.9 ± 0.8 |
| 695 | 3.73 | 0.00233 | 0.014 | 2.35 | 80.53 | 0.18 | 34.0 ± 1.8 |
| 740 | 3.90 | 0.00350 | 0.012 | 1.46 | 72.49 | 0.10 | 32.1 ± 3.2 |
| 800 | 4.18 | 0.00494 | 0.041 | 1.10 | 64.28 | 0.24 | 30.5 ± 4.3 |
| Fusion | 4.85 | 0.00442 | 0.081 | 2.55 | 72.41 | 0.53 | 39.8 ± 1.2 |
| Total | 0.00 | 143 | 0.016 | 100.00 | 88.02 | 0.38 | 36.5 ± 0.6 |
| Total without 695°C-Fusion | | | | 92.54 | | | 36.7 ± 0.5 |
| **Sanidine** | | | | | | | |
| **Sample TJ-77-88: J = 0.010020** | | | | | | | |
| 700 | 2.76 | 0.00262 | 0.112 | 9.99 | 72.04 | 1.16 | 35.6 ± 0.4 |
| 800 | 1.95 | 0.00017 | 0.052 | 17.29 | 97.36 | 8.46 | 33.9 ± 0.1 |
| 850 | 1.94 | 0.00013 | 0.040 | 16.73 | 97.90 | 8.44 | 34.0 ± 0.1 |
| 890 | 1.95 | 0.00012 | 0.034 | 19.36 | 97.95 | 7.48 | 34.1 ± 0.1 |
| 930 | 1.96 | 0.00016 | 0.031 | 10.25 | 97.38 | 5.24 | 34.2 ± 0.2 |
| 970 | 1.99 | 0.00026 | 0.029 | 13.19 | 95.92 | 3.02 | 34.2 ± 0.2 |
| 1020 | 2.09 | 0.00054 | 0.030 | 10.16 | 92.22 | 1.51 | 34.5 ± 0.2 |
| 1100 | 2.47 | 0.00188 | 0.041 | 1.94 | 77.33 | 0.60 | 34.2 ± 1.0 |
| Fusion | 3.18 | 0.00474 | 0.058 | 1.08 | 55.94 | 0.33 | 31.9 ± 1.8 |
| Total | 2.07 | 0.00053 | 0.045 | 100.00 | 93.49 | 5.54 | 34.3 ± 0.2 |
| Total without 700, 1100°C and fusion | | | | 86.99 | | | 34.1 ± 0.1 |

*measured. [c]corrected for post-irradiation decay of $^{37}Ar$ (35.1 day 1/2-life). [+]$[^{40}Ar_{tot.} - (^{36}Ar_{atmos.})(295.5)] / {}^{40}Ar_{tot.}$

**calculated using correction factors of Dalrymple et al. (1981); two sigma, intralaboratory errors.

## Table 2

## $^{36}AR/^{40}AR$ vs. $^{39}AR/^{40}AR$ Isotope Correlations Using Plateau Analytical Data from Incremental Heating Experiments on Minerals fromVolcanic Units in the East Tintic Mountains, Utah.

| Sample (Ma)* | Isotope Correlation Age (Ma)*** | $^{40}Ar/^{36}Ar$ Intercept** | MSWD | % of Total $^{39}Ar$ | Calculated $^{40}Ar/^{39}Ar$ Plateau Age |
|---|---|---|---|---|---|
| **Biotite** | | | | | |
| TJ-8-87 | 34.7 ± 0.2 | 326.8 ± 26.3 | 1.84 | 81.28 | 37.4 ± 0.3 |
| TJ-112-88 | 34.7 ± 0.1 | 352.2 ± 33.1 | 1.58 | 88.84 | 35.3 ± 0.1 |
| TJ-84-88 | 34.2 ± 0.1 | 322.6 ± 21.3 | 0.14 | 97.24 | 34.5 ± 0.2 |
| HS-UTH-86-2 | 33.0 ± 0.2 | 323.2 ± 26.1 | 0.17 | 89.78 | 33.6 ± 0.2 |
| **Muscovite** | | | | | |
| KS-2A-87 | 36.6 ± 0.2 | 346.3 ± 31.3 | 0.19 | 92.54 | 36.7 ± 0.5 |
| **Sanidine** | | | | | |
| TJ-77-88 | 34.0 ± 0.1 | 360.3 ± 42.6 | 0.43 | 86.99 | 34.1 ± 0.1 |

* Calculated using the inverse abscissa intercept ($^{40}Ar/^{39}Ar$ ratio) in the age equation.
** Inverse ordinate intercept.
*** Table 1.

graphically unresolvable exsolution or compositional zonation within constituent biotite grains; and/or, 3) intracrystalline inclusions. Gas increments evolved during most intermediate-temperature increments are characterized by mutually similar apparent K/Ca ratios, indicating experimental evolution of gas from compositionally uniform populations of intracrystalline sites. Apparent ages recorded by intermediate-temperature increments evolved from each of the biotite concentrates are similar and yield well-defined plateau ages. The plateau analytical data yield similar isotope correlations ages indicating a lack of significant extraneous argon contamination. Because of these relationships, the biotite plateau ages are considered geologically meaningful.

Low- and intermediate-temperature portions of the muscovite analysis are characterized by generally uniform apparent K/Ca ratios indicating experimental evolution of gas from a compositionally uniform population of intracrystalline sites. The higher temperature gas fractions display markedly fluctuating apparent K/Ca ratios which likely reflect experimental evolution of gas from minor, optically undetectable mineralogical contaminates in the muscovite concentrate. The low- and intermediate temperature increments yield a well-defined plateau age which is similar to that resulting from isotope correlation of the plateau data. This suggests the muscovite plateau age is geologically meaningful.

Consistent intrasample variations in apparent K/Ca ratios in low- and intermediate-temperature portions of the sanidine analysis suggests that compositionally variable intracrystalline sites contributed gas during the experiment. However, most of these increments record similar apparent ages which define a plateau. These data yield a similar isotope correlation age indicating the sanidine plateau age may be considered geologically reliable.

### Revised Volcanic and Intrusive Sequence

Mapping in the central East Tintic Mountains indicates the occurrence of several significant sedimentary and volcanic units not recognized by Morris and Lovering (1979) or Morris (1975). For example, two lacustrine sedimentary horizons are intercalated with ash-flow tuff and flow/agglomerate members of the Copperopolis Latite. The lower sedimentary horizon (0-50 m) overlies an ash-flow tuff member (the upper portion of which is moderately reworked) and consists dominantly of fissile shale with lesser amounts of mudstone and volcaniclastic sandstone. The coarser-grained horizons in this unit generally contain the greater amount of carbonate cement. Small (~1 cm), primary ovoidal structures in the shaley horizons probably represent calcareous gastropod shells which have been replaced by pyrite and subsequently converted to limonite.

The upper lacustrine horizon is separated from the lower by a previously unmapped flow and agglomerate member of the Copperopolis Latite. The agglomerate often contains deformed clasts of shale or mud (between large blocks) that were apparently ripped up from the lake bottom during deposition. The flows which occupy this stratigraphic position near Sunrise Peak appear to have vented from the Sunrise Peak Stock (as first suggested by Lindgren and Laughlin, 1919) and dikes of similar composition to the north. Consequently, this

## Table 3
## Fission Track Age Data

| Sample Number | Mineral Analyzed | Method | Location N. Lat. W. Long. | No of Grains | Track Denisty tr/cm² 10⁵ Fossil | Induced | Neutron Dose D/cm² x 10¹⁴ | Age ± Error (2 ) |
|---|---|---|---|---|---|---|---|---|
| TJ-6 | Apatite | Pop. | 39°51'11" 111° 3'20" | 150 | 1.30 (701) | 2.44 (1315) | 11.26 (3121) | 35.8 ± 5.1 Ma |
| TJ-9 | Apatite | Pop. | 39°51'11" 111° 3'20" | 150 | 1.92 (1038) | 3.44 (1860) | 11.26 (3121) | 37.5 ± 5.2 Ma |

unit is informally referred to as the flows and agglomerates of Sunrise Peak (Keith et al., 1989b). The upper lacustrine horizon (0-20 m) overlies a few meters of finer, reworked volcanic material and consists of alternating beds of organic-rich shale (abundant plant remains) and limestone (0-3 m).

Fission-track dating of apatites extracted from the volcaniclastic material in each of the two lacustrine horizons yields an approximate age of about 36-37 m.y. (Table 3) for this episode of volcanism and sedimentation. In addition, $^{40}Ar/^{39}Ar$ ages for biotite from a biotite latite vitrophyre (sample # TJ-8; 37.4 ± 0.3 Ma) and sericite from the lower lacustrine horizon (sample # KS-2A; 36.7 ± 0.5 Ma; Figure 2) suggest approximately the same ages for some of the volcanic and intrusive units beneath the lacustrine horizons. Biotite from a Sunrise Peak dike (sample # TJ-112), which presumably fed the flows and agglomerates between the two major lacustrine horizons, yielded a $^{40}Ar/^{39}Ar$ age of 35.3 ± 0.1 Ma. These ages are significantly older than the 32 m.y. age suggested by Morris and Lovering (1979) for these volcanic rocks, but they are in accordance with the recently determined ages of volcanic rocks found in adjacent ranges to the south, east, and west (Hannah and Macbeth, 1989; Witkind and Marvin, 1989; Le Vot, 1984; Villien, 1984; Willis, 1986).

The upper lacustrine horizon may grade into an epiclastic sedimentary unit consisting of volcanic conglomerates and sandstones with a variety of latitic clast compositions. Due to the high porosity and carbonate content of the epiclastic sedimentary rocks, hydrothermal fluids more completely altered these sedimentary rocks compared to subjacent and overlying latite flows. However, in a few of the less-altered outcrops of this unit, abundant pumice (partly replaced by calcite) is interspersed with latite breccia. Some outcrops of this unit also contain a few angular clasts of Tintic Quartzite and other Paleozoic carbonates. The distribution and composition of this unit suggest it occurred near a sharp transition from a quiet lacustrine environment to a higher relief terrane with some Paleozoic rocks still exposed at the surface - possibly along a caldera wall.

Following deposition of the upper lacustrine unit and the epiclastic sediments, widespread lava flows occurred, which range in composition from latite to shoshonite (Table 4). At least 6 flows can be distinguished in a few well exposed areas, but mapping individual flows is generally not possible due to the near identical composition of most flows. The reciprocal abundance of biotite versus orthopyroxone is perhaps the best field criteria we used for distinguishing the biotite latite flow units from the orthopyroxene-bearing mafic (or shoshonite) flows, which contain only traces of oxidized, resorbed biotite. Both units contain abundant clinopyroxene, plagioclase, and titanomagnetite and are clearly genetically related.

In addition, the distribution and thickness of these flows and sedimentary units may be controlled to some extent by an earlier-formed caldera, possibly related to eruption of the tuff member of the Copperopolis Latite. For example, the mafic flows pinch out to the northeast of our mapped area, but thicken dramatically to the southwest (Keith et al., 1989b). Lindgren and Loughlin (1919) described the occurrence of olivine basalt dikes west of Tintic Mountain while Morris and Lovering (1979) stated that they failed to find any evidence of this lithology. Lindgren and Loughlin (1919) report a partial chemical analysis of a flow near Buckhorn Mountain which is more alkaline and mafic than any rocks found by Morris and Lovering (1979), but is chemically similar to the mafic flows we have analyzed (Table 4).

Several vitrophyre horizons were located at the base of some of the biotite latite flows and were extensively sampled. Contrary to previous descriptions of these rocks, we found that many of the fresh flows and vitrophyres also contained phenocrystic amphibole and magmatic sulfide blebs. The occurrence of amphibole in some flows or samples and its absence in others is analogous to the reciprocal abundance of biotite and orthopyroxene. For example, the amphibole often occurs as overgrowths on, or as partial ("fibrous") replacements of, clinopyroxene. In other instances, clinopyroxene is found as a reaction rim on amphibole; the more oxidized or degassed lavas less commonly contain amphibole. These relationships suggest that amphibole occurred only late in the crystallization sequence and was often removed from the magma during degassing.

The biotite latite dikes have essentially the same

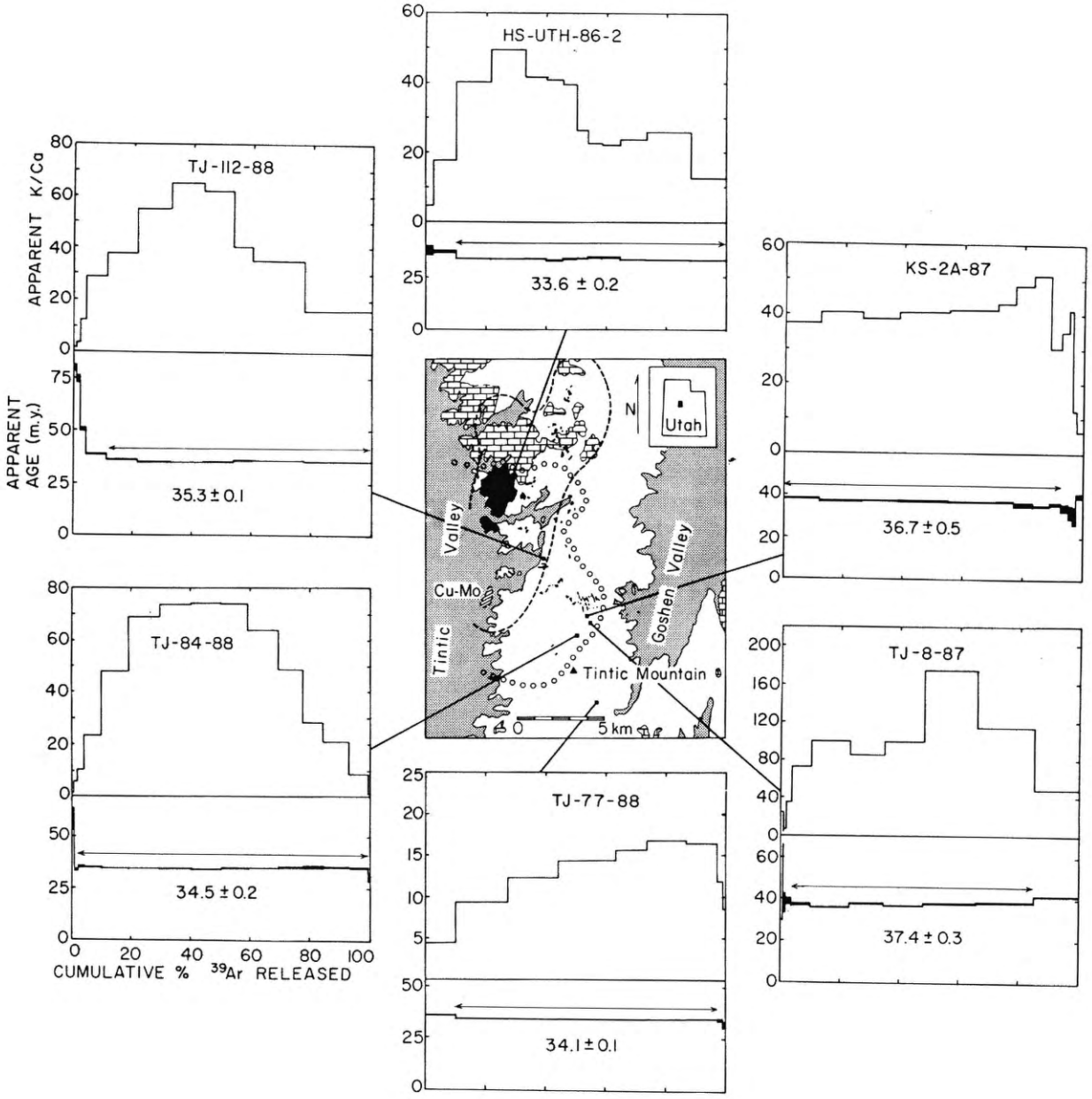


Fig.2. $^{40}Ar/^{39}Ar$ age and apparent K/Ca spectra of biotite, muscovite, and sanidine concentrates from the East Tintic Mountains. Two-sigma intralaboratory uncertainties indicated by vertical width of bars. Experimental temperatures of argon evolution increase from left to right. Total gas or plateau ages (plateau increments outlined by arrows) listed on each spectrum. On the central index map, replacement and vein ore deposits occur in the area surrounded by the dashed line. The eastern lobe of this area comprises the East Tintic mining district; the remainder comprises the Tintic district. Ore-related monzonite intrusions are shown as solid black; all other Tertiary intrusions and volcanic rocks in the East Tintic Mountains are shown in white; the brick pattern represents Precambrian and Paleozoic sedimentary rocks; Quaternary valley-fill sediments are shown as stipple. The immediate vicinity of the sub-economic Cu-Mo deposit is covered by alluvium or mapped by others (Hannah and Macbeth, 1990). The area enclosed by the trail of circles contains nested calderas and related lacustrine sediments and abundant intrusions, Keith et al., 1989b).

chemical and modal composition as the biotite latite flows, including the occurrence of amphibole and magmatic sulfide blebs (discussed later). The dikes are classified as latite due to the extremely fine-grained texture of the groundmass. Inasmuch as most of the flow and lacustrine units dip about 20° to the southeast, these dikes are progressively eroded to a deeper level going from the southeast to the northwest portion of our mapped area. As this is done, the groundmass texture of the dikes becomes coarser grained. This transition along

# Table 4
## Whole-Rock Major Element Analyses

| Sample # | * | * | TJ-84 | TJ-76 | TJ-80A | TJ-80B |
|---|---|---|---|---|---|---|
| Lithology | Silver City Monzonite | Sunrise Peak Monzonite | Biotite Latite Dike | Upper Biotite Latite | Upper Biotite Latite | Upper Biotite Latite |
| Wt % Oxide | | | | | | |
| $SiO_2$ | 61.08 | 60.13 | 59.02 | 59.41 | 58.68 | 60.83 |
| $TiO_2$ | 0.89 | 0.89 | 0.94 | 1.01 | 0.99 | 0.99 |
| $Al_2O_3$ | 16.14 | 16.19 | 16.64 | 16.60 | 16.22 | 17.51 |
| $Fe_2O_3$ | 7.59 | 7.16 | 7.00 | 7.58 | 8.25 | 6.48 |
| MnO | 0.12 | 0.14 | 0.12 | 0.12 | 0.12 | 0.12 |
| MgO | 2.21 | 2.84 | 2.50 | 2.75 | 3.10 | 1.79 |
| CaO | 3.97 | 4.16 | 5.02 | 5.64 | 5.94 | 5.51 |
| $Na_2O$ | 3.08 | 3.20 | 3.61 | 2.57 | 2.62 | 2.59 |
| $K_2O$ | 4.50 | 4.88 | 4.55 | 3.90 | 3.64 | 3.72 |
| $P_2O_5$ | 0.43 | 0.40 | 0.48 | 0.40 | 0.43 | 0.45 |
| S | 0.02 | 0.02 | 0.06 | 0.01 | 0.01 | 0.01 |
| CIPW Norm | | | | | | |
| Q | 15.39 | 10.83 | 9.18 | 14.57 | 14.47 | 18.37 |
| C | 0.03 | 0.00 | 0.00 | 0.00 | 0.00 | 0.30 |
| Or | 26.58 | 28.81 | 26.91 | 23.04 | 21.49 | 21.96 |
| Ab | 26.03 | 27.09 | 29.81 | 21.64 | 22.13 | 21.87 |
| An | 16.87 | 15.42 | 16.14 | 22.30 | 21.77 | 24.41 |
| Di | 0.00 | 2.02 | 2.21 | 2.36 | 1.48 | 0.00 |
| Hy | 5.50 | 6.14 | 5.21 | 5.76 | 7.03 | 4.45 |
| Mt | 0.00 | 0.00 | 0.00 | 0.00 | 0.00 | 0.00 |
| Il | 0.21 | 0.26 | 0.25 | 0.27 | 0.27 | 0.26 |
| Hm | 7.59 | 7.16 | 7.00 | 7.58 | 8.25 | 6.48 |
| Tn | 0.00 | 1.83 | 1.99 | 2.14 | 2.09 | 0.00 |
| Ru | 0.78 | 0.00 | 0.00 | 0.00 | 0.00 | 0.85 |
| Ap | 1.02 | 0.95 | 1.13 | 0.96 | 1.03 | 1.06 |
| Pr | 0.04 | 0.04 | 0.00 | 0.00 | 0.00 | 0.00 |
| Diff. Index | 68.00 | 66.73 | 65.90 | 59.25 | 58.09 | 62.19 |

### Whole-Rock Major Element Analyses

| Sample # | TJ-8 | TJ-64 | TJ-75 | TJ-77 | * | * |
|---|---|---|---|---|---|---|
| Lithology | Lower Biotite Latite | Lower Biotite Latite | Rhyolite Of Keystone Springs | Rhyolite Of Keystone Springs | Swansea Quartz Monzonite | Packard Quartz Latite |
| Wt % Oxide | | | | | | |
| $SiO_2$ | 60.39 | 58.47 | 71.49 | 70.45 | 71.63 | 70.86 |
| $TiO_2$ | 0.93 | 0.99 | 0.42 | 0.42 | 0.42 | 0.40 |
| $Al_2O_3$ | 16.24 | 17.47 | 14.92 | 15.55 | 14.73 | 15.42 |
| $Fe_2O_3$ | 7.25 | 6.91 | 2.05 | 2.28 | 2.34 | 2.44 |
| MnO | 0.12 | 0.12 | 0.09 | 0.10 | 0.07 | 0.06 |
| MgO | 2.61 | 2.42 | 0.65 | 0.56 | 0.71 | 0.70 |
| CaO | 5.19 | 5.50 | 1.05 | 1.22 | 1.14 | 2.62 |
| $Na_2O$ | 2.50 | 2.99 | 3.90 | 4.32 | 3.03 | 3.19 |
| $K_2O$ | 4.30 | 4.61 | 5.35 | 5.02 | 5.82 | 4.17 |
| $P_2O_5$ | 0.44 | 0.49 | 0.08 | 0.10 | 0.12 | 0.14 |
| S | 0.01 | 0.01 | 0.01 | 0.00 | 0.01 | 0.01 |
| CIPW Norm | | | | | | |
| Q | 15.71 | 10.30 | 25.34 | 22.95 | 28.61 | 30.06 |
| C | 0.00 | 0.00 | 1.00 | 1.03 | 1.67 | 1.23 |
| Or | 25.39 | 27.23 | 31.61 | 29.64 | 34.37 | 24.63 |
| Ab | 21.05 | 25.06 | 33.01 | 36.54 | 25.60 | 27.02 |
| An | 20.45 | 20.78 | 4.66 | 5.43 | 4.88 | 12.10 |
| Di | 1.88 | 0.29 | 0.00 | 0.00 | 0.00 | 0.00 |
| Hy | 5.62 | 5.90 | 1.63 | 1.39 | 1.76 | 1.75 |
| Mt | 0.00 | 0.00 | 0.00 | 0.00 | 0.00 | 0.00 |
| Il | 0.26 | 0.27 | 0.17 | 0.21 | 0.13 | 0.11 |
| Hm | 7.25 | 6.91 | 2.05 | 2.28 | 2.34 | 2.44 |
| Tn | 1.70 | 2.08 | 0.00 | 0.00 | 0.00 | 0.00 |
| Ru | 0.09 | 0.00 | 0.33 | 0.31 | 0.35 | 0.34 |
| Ap | 1.05 | 1.16 | 0.19 | 0.23 | 0.29 | 0.32 |
| Pr | 0.00 | 0.00 | 0.02 | 0.00 | 0.02 | 0.02 |
| Diff. Index | 62.15 | 62.59 | 89.96 | 89.13 | 88.58 | 81.71 |

### Whole-Rock Major Element Analyses

| Sample #TJ-108 | TJ-18 |
|---|---|
| Lithology | Upper Biotite Latite | Mafic flows |
| Wt % Oxide | | |
| $SiO_2$ | 62.02 | 54.23 |
| $TiO_2$ | 0.83 | 1.16 |
| $Al_2O_3$ | 15.84 | 17.71 |
| $Fe_2O_3$ | 6.45 | 8.46 |
| MnO | 0.09 | 0.14 |
| MgO | 2.51 | 2.57 |
| CaO | 4.37 | 7.69 |
| $Na_2O$ | 3.10 | 3.46 |
| $K_2O$ | 4.43 | 3.93 |
| $P_2O_5$ | 0.36 | 0.57 |
| S | 0.12 | 0.04 |
| CIPW Norm | | |
| Q | 15.62 | 3.57 |
| C | 0.00 | 0.00 |
| Or | 26.15 | 23.24 |
| Ab | 26.21 | 28.66 |
| An | 16.26 | 21.51 |
| Di | 0.08 | 7.34 |
| Hy | 6.23 | 2.99 |
| Mt | 0.00 | 0.00 |
| Il | 0.00 | 0.29 |
| Hm | 6.45 | 8.46 |
| Tn | 2.12 | 2.46 |
| Ru | 0.00 | 0.00 |
| Ap | 0.85 | 1.35 |
| Pr | 0.21 | 0.00 |
| Diff. Index | 67.98 | 55.47 |

some dikes includes a change to Silver City Monzonite. Near this transition, the latite or monzonite oftens contains fragments or blocks (up to 3 m) of Tintic Quartzite. The biotite latite dikes often contain broken phenocrysts and strong flow foliation due to rapid eruption rates; the Silver City Monzonite may represent a more passively emplaced comagmatic batch of magma, which accounts for the numerous stoped blocks in the Silver City Stock (Morris and Lovering, 1979) and in satellite intrusions which we mapped.

The field evidence for correlating the biotite latite dikes and the Silver City Stock as being comagmatic is supported by the $^{40}Ar/^{39}Ar$ ages of each unit. For example, a "vitrophyre" sample (TJ-84) from a vent facies biotite latite dike exhibits an age of 34.5 ± 0.2 Ma. Our plateau age for biotite from the Silver City Stock (sample HS-UTH-86-2; courtesy of J. Hannah) is only slightly younger, 33.6 ± 0.2 Ma (Tables 1 and 2; Figure 2).

Monzonite porphyry of Silver City Stock lithology extends south and east (Figure 1) across most of our mapped area. The correlation of these intrusions with the Silver City Stock is tentatively made on the basis of similar modal compositions and textures. Morris (1975) located some of these intrusions, but classified most of them as monzonite of Sunrise Peak lithology. The major element compositions of these two monzonites are essentially indistinguishable (Table 4). The apparent traditional criteria for distinguishing these two lighologies appears to be based on the occurrence of amphibole and a coarser-grained groundmass in the Silver City Monzonite.

Near the extreme southern end of the mapped area on the east flank of Tintic Mountain, a dome or neck of feldspar porphyry was encountered. This lithology is identical in chemical and mineralogical composition to the descriptions of Lindgren and Laughlin (1919) of the rhyolite of Tintic Mountain. In addition, it is chemically almost identical to the Swansea Quartz Monzonite and the Packard Quartz Latite (Table 4). Its most obvious characteristics are large Carlsbad-twinned sanidine phenocrysts (up to 3 cm) and an absence of any phenocrystic quartz. Smaller phenocrysts of plagioclase and minor biotite, oxyhornblende, titanomagnetite, and traces of magmatic pyrrhotite are also present. Lindgren and Laughlin (1919) stated that this lithology occurs on the west flank of Tintic Mountain, whereas the largest outcrop we found is on the east flank. However one small intrusion occurs on the west flank (Keith et al., 1989b) which is nearly correlative in modal composition, but contains a slightly higher proportion of biotite and oxidized, relict amphibole. This unit is informally referred to as the rhyolite of Keystone Springs to avoid use of the term "Tintic Mountain" which has been widely applied to other rock types. Water-clear sanidine from this unit yielded a $^{40}Ar/^{39}Ar$ age of 34.1 ± 0.1 Ma (Figure 2, Tables 1 and 2).

### Magmatic Sulfides

Immiscible magmatic sulfide blebs occur in vitrophyres of several biotite latite flows and dikes of the same composition. Very fresh samples of the rhyolite of Keystone Springs also have traces of magmatic pyrrhotite. The abundance and diameters of sulfide blebs between various units varies widely. The most sulfide-rich biotite latite glass from the East Tintic Mountains which has been found so far contains globules up to 450 microns in diameter with a modal abundance of 0.02% (Figure 3). Careful modal analysis of the sulfide distribution in one sample revealed a total of 465 sulfide blebs over 1 micron in size in one thin section. Titanomagnetite contained 36% of the blebs, clinopyroxene contained 27%, the matrix 22%, biotite 10%, and plagioclase contained only 4%. The associated glass has S concentrations (~400 ppm) anticipated for sulfide saturation of this bulk composition (Carroll and Rutherford, 1985).

By comparison, several vitrophyres are relatively sulfide-poor. Standard petrographic thin sections of such vitrophyres commonly contain fewer than 10 sulfide blebs with diameters in the range of 1-10 microns. In addition, there are no "degassed sulfide blebs" (as described later) which might indicate that these vitrophyres were at one time more sulfide-rich. Petrography and major-element analysis clearly suggest that some flows were sulfide-rich (i.e. TJ-84 and TJ-55) and others of the same bulk composition were sulfide-poor (i.e. TJ-8, TJ-64, and TJ-80A; Table 3). Sulfide-poor flows are found both stratigraphically above and beneath the sulfide-rich flows.

Some vitrophyres which are present along chilled dike margins also contain magmatic sulfides. Recent mapping reveals that monzonite intrusions of the productive Silver City lithology are far more wide-spread to the east and south of the stock (compare Figure 1A and 1B) than previous maps have indicated (Morris, 1975). Monzonite intrusions near the southern part of the mapped area begin to give way to biotite latite dikes (along the same zones of emplacement) as the paleosurface at the time of intrusion is approached. Some portions of these biotite latite dikes were chilled rapidly enough that glass (now variably hydrated or devitrified) was preserved. These glassy or microcrystalline samples contain the highest proportion of magmatic sulfides. The reason for this unusual sulfide preservation may have been because the dikes were chilled, but not lowered completely to atmospheric pressure. By analogy, quenched glasses from submarine basalts (> 1000 m water depth) are notable for preserving high sulfur contents and sulfide globules indicative of magmatic conditions.

The sulfide blebs, present in both flow vitrophyres and dikes, are composed of pyrrhotite, pyrite, As-rich pyrite, chalcopyrite, cubanite, and "Fe-oxide". The pyrrhotite, pyrite, chalcopyrite, and cubanite, are the earliest exsolved components of the sulfide blebs which are still preserved (Figure 3). As-rich pyrite and Fe oxide result from degassing of the sulfide bleb after eruption or emplacement in shallow dikes (as discussed later).

The preliminary analytical data of Tintic magmatic pyrrhotites indicates that a small amount of compositional variation occurs due to reaction with their surrounding host mineral. Pyrrhotites hosted by titanomagnetite are distinctly more Fe-rich (Fe/S ratio of 0.90 t0 0.94) than those hosted by clinopyroxene or plagioclase (Fe/S ratio of 0.90 to 0.84). Microprobe analysis of the minor elements in the sulfides (Figure 4) indicates the expected high concentrations of Ni (max. of 0.96 wt. % and ave. of 0.40 wt. %) and Co (max. of

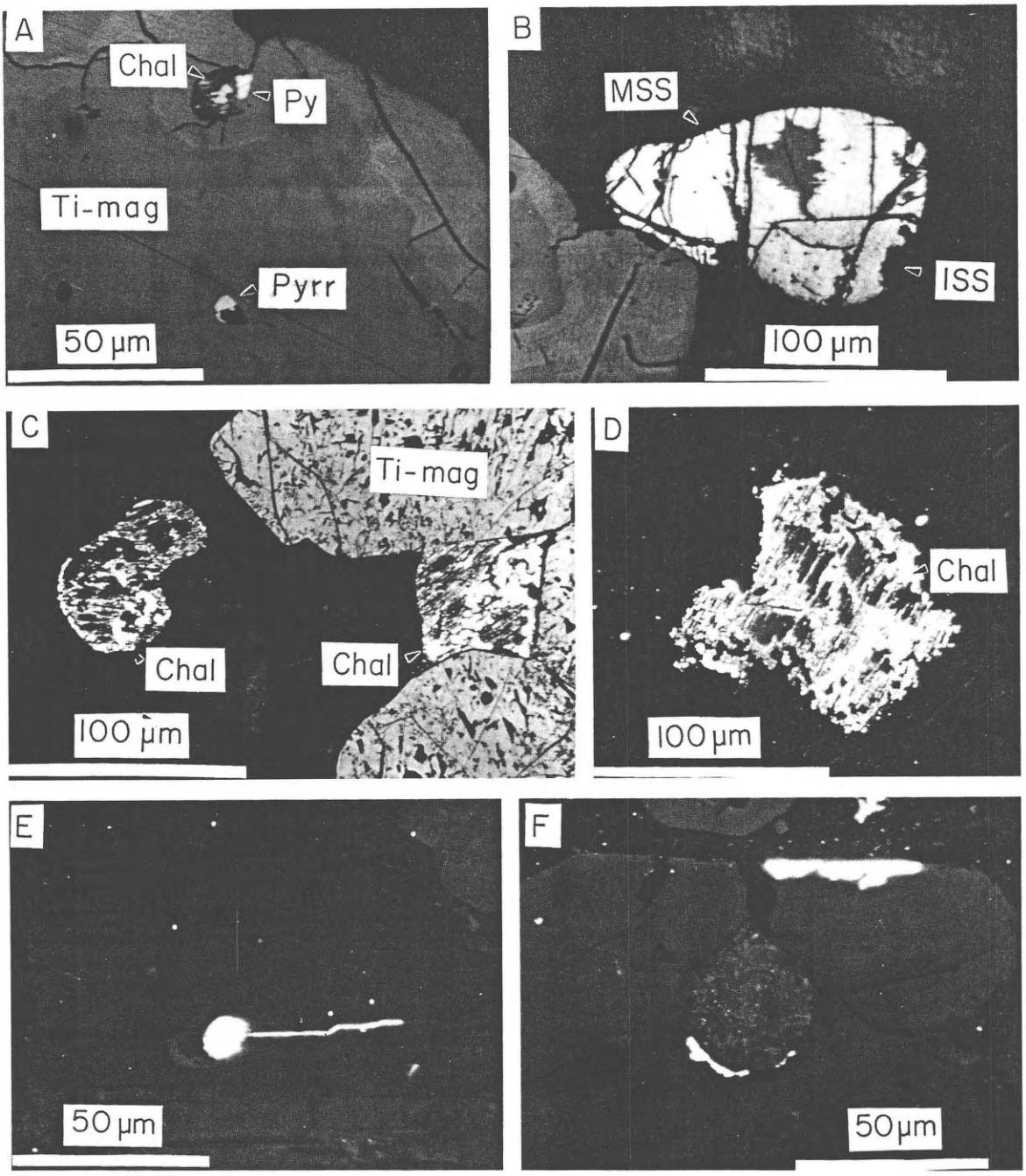


Fig. 3. Photomicrographs of exsolved and degassed magmatic sulfides from a biotite latite dike (TJ-84) and a lava vitrophyre (TJ-55). A. Comparison of two magmatic sulfide blebs locked within a single titanomagnetite grain (TJ-55). As the margin of the titanomagnetite and the upper sulfide bleb react with the oxygen in the cooling lava vitrophyre, titanomagnetite oxidizes to become maghemite and the pyrrhotite oxidizes to pyrite, Fe oxide, and chalcopyrite. Pyrrhotite sequestered towards the interior of the bleb is not oxidized. B. Reflected light photomicrograph of an exsolved composite magmatic sulfide bleb present in a glomeroporphyritic clot from a biotite latite flow vitrophyre (TJ-55). This composite magmatic sulfide grain is 140 microns in length and consists mainly of three phases: chalcopyrite (ISS), Ni-Co-bearing pyrite (MSS), and a small degassed Fe-oxide core (gray). Not apparent in this photo are small exsolved phases of cubanite in the chalcopyrite and Ni-rich zones in the pyrite. The grain is surrounded mostly by glass. Distler et al. (1986) describe amazingly similar sulfide blebs present in oceanic basalts in which the sulfide bleb has segregated into two halves; one half is a Ni-bearing MSS and the other half is close to cubanite in composition. Lightfoot et al. (1984) note very similar magmatic sulfide globules in the Insizwa Cu-Ni deposit except the Cu-rich half is dominantly chalcopyrite as in this illustration. C. These two magmatic sulfide blebs are composed mostly of pyrite (white lines), interstial Fe-oxide (gray), surrounded by a partial rim of exsolved chalcopyrite (white). The largest white areas within the blebs are also chalcopyrite. The bleb on the left, surrounded by glass exhibits a rounded shape whereas the bleb on the right has molded to fit between three titanomagnetite grains. D. Very similar sulfide bleb to the two illustrated in part C, except it shows marginal resorption. The most prominent white areas of the bleb are chalcopyrite, the gray is Fe oxide and the white lines are pyrite. E. Small magmatic sulfide bleb enclosed within biotite adjacent to a smaller melt inclusion. The sulfide bleb degassed along biotite cleavage forming a lamellae of As-rich pyrite (bright white) which does not extend to the margin of the biotite phenocryst. F. Completely degassed magmatic sulfide bleb hosted by a euhedral clinopyroxene phenocryst. The spherical bleb is now composed of Fe oxide while adjacent portions of the clinopyroxene have been replaced by As-rich pyrite (bright white).

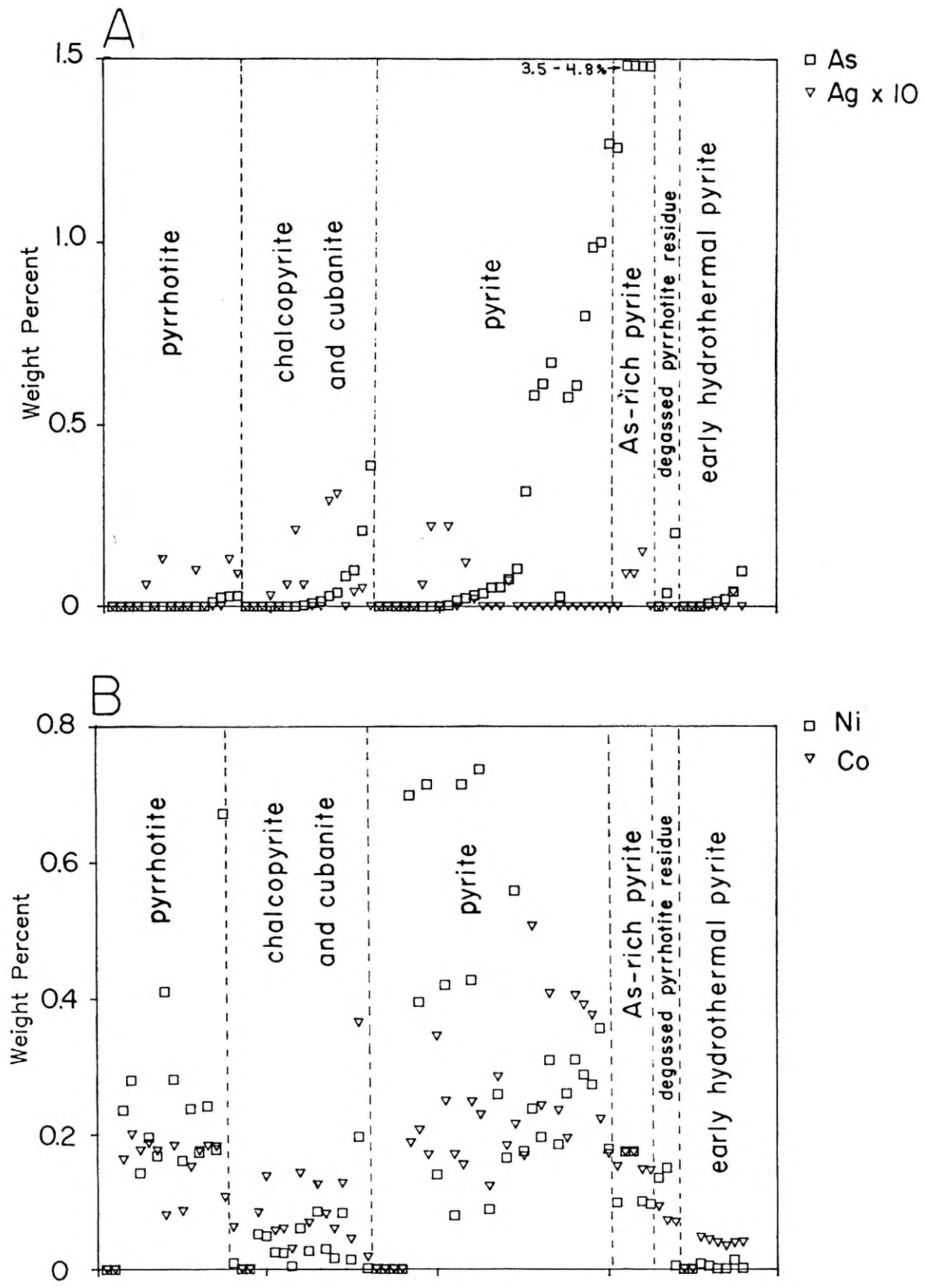


Fig. 4. Minor element content of sulfides plotted versus different sulfide occurrences: A) As and Ag(X10) abundances; B) Ni and Co abundances. Analyses are ordered along the x-axis according to increasing As content within each group. The "early hydrothermal pyrite" is pyrite disseminated in the intensely altered lacustrine sedimentary rocks.

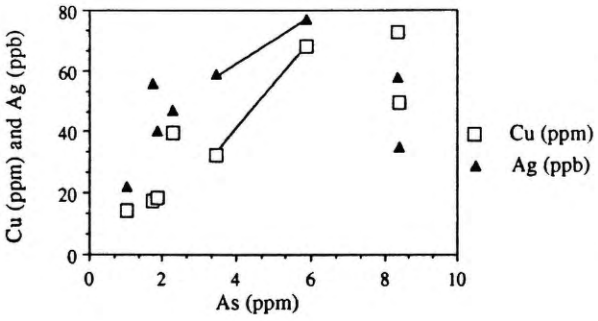


Fig. 5. Scatter plot of As versus Cu and Ag contents of latites and monzonites from the central East Tintic Mountains. See text for discussion of data.

0.51 wt. % and ave. of 0.14 wt. %); however, the weighted average Cu and Ag contents of the blebs may be particularly high (Cu max. of 34.7 wt. % and ave. of 5.50 %; Ag max. of 0.03 % and ave. of < 0.02 %) when compared to magmatic sulfides from other systems.

Inasmuch as argentian pentlandite has been noted in some magmatic sulfides from other localities, it was deemed advisable to analyze the magmatic sulfides for detectable Ag; this effort yielded limited success. All Ag "anomalies" found were only just above background. The Ag anomalies were generally reproducible, but no consistent Ag-bearing phase was verified. The apparent Ag anomalies were found in heterogeneous magmatic sulfides, but none was found in hydrothermal pyrite analyzed at the same time (Figure 4; which suggests the anomalies may be real). ICP analysis of several acid leachates from these samples (Figure 5) yields approximately the same Cu/Ag ratio as calculated using modal estimates of relative sulfide abundances and the microprobe analyses. Consequently, the magmatic sulfides may contain detectable Ag, but much work remains to be done to verify or refute this possibility.

The textures and inclusion relationships of the sulfide blebs correspond to what might be expected for exsolved and degassed magmatic sulfides. The precursor of the Cu-sulfides is interpreted to be a non-stoichiometric Cu-Fe-S phase (ISS) which exsolves from the sulfide bleb at high temperatures (>500° C). The relict exsolved ISS blebs form a scalloped margin around the parental monosulfide grain, line early-formed fractures (Figure 3C and 3D), or occur as a single discreet grain bounded by a curved surface (Figure 3A and 3B). [Hildreth (1977) also found Cu-rich margins on the much smaller pyrrhotite grains in the Bishop Tuff.] The presence of small inclusions of cubanite in chalcopyrite suggests that at lower temperatures the ISS phase exsolves chalcopyrite and very minor cubanite.

The remaining Ni-Co-bearing pyrrhotite and pyrite are often heterogeneous in Ni content (Figure 4). This may be related to a migration process analogous to pentlandite exsolution. However, no pentlandite has been found in any sulfide blebs. The Ni-rich, As-poor pyrite which is present in the blebs may have exsolved from sulfur-rich MSS and was formed from the MSS after eruption or intrusion. This may be due in part to the fact that S-rich pyrrhotite compositions spontaneously exsolve upon quenching, as noted by Craig and Scott (1974). Evidence for the occurrence of this process in calc-alkaline volcanic rocks was also encountered by Whitney (1984) during examination of pyrrhotite blebs in the Fish Canyon Tuff.

Pyrrhotite in the magmatic blebs is rarely preserved unless the blebs are embedded: 1) near the centers of silicate phenocrysts (which are devoid of cracks to the crystal surface), 2) within titanomagnetite devoid of oxidation exsolution (or maghemitization) or 3) within some glomeroporphyritic clots. When these conditions are *not* met, the pyrrhotite apparently degasses to form As-rich pyrite, Fe-oxide, and a sulfurous gas (Figure 3E and 3F).

In dike samples, it is noteworthy that S and As apparently migrate to the margins of the pyrrhotite crystal along a prefered crystallographic direction (relict {0001} planes in hexagonal pyrrhotite?). Magmatic sulfide blebs present in lava vitrophyre samples show only minor evidence of crystallographic control during degassing of S and As; loss of S and As occurs along cracks in the bleb (Figure 3B). The end result of this degassing process in both vitophyres and dikes is an Fe oxide residue with an Fe/O ratio slightly lower than hematite. Some samples intermediate in texture between latite and monzonite exhibit spherical "spongy" Fe oxides where >90 % of the magmatic sulfur has been removed by degassing processes (Figure 3F). The size, distribution, and modal abundance of the "spongy" Fe oxides mimics the occurrence of the magmatic sulfides. The Co and Ni content of the Fe oxide residue is approximately the same as the original pyrrhotite (Figure 4). The Fe and S distribution in a complexly degassed sulfide bleb (very similar to Figures 3C and 3D), consisting of intermixed As-rich pyrite, pyrite, and Fe oxide, was mapped using a microprobe X-ray mapping technique (Keith, in prep.). The results show a very homogenous distribution of Fe and very inhomogenously distributed S and As. Consequently, Fe, Co, and Ni show little evidence of mobility during this degassing process.

### Hydrothermal Alteration

Within the mapped area, an extensive area of hydrothermally altered volcanic rocks occurs which is approximately coincident with a swarm of dikes and small intrusions of Silver City Monzonite lithology (Figure 1). No previous maps or reports have delineated or described the alteration, probably because of the apparent lack of nearby mineralization. However, the character of the alteration exhibits several similarities to the well-studied alteration in the East Tintic District that is present around productive intrusions (Lovering, 1949) and, consequently, merits some description and analysis.

The hydrothermal alteration was apparently structurally and chemically controlled in several ways (Kim and Keith, 1989). The poorly welded tuff member of the Copperopolis Latite (at the base of the stratigraphic section) exhibits a pervasive argillic alteration. Whether or not the argillic alteration is zoned exclusively around monzonite intrusions or is related in part to fractures and faults is not well known. The high porosity and permeability of the tuff apparently allowed wider dispersal of alteration than occurred in other rock types.

The most obvious zonation of hydrothermal alteration is caused by stratigraphic changes in lithology. For example, immediately above the argillically altered tuff member of the Copperopolis Latite, the sedimentary rocks of the lower member of the Golden's Ranch Formation commonly record a distinct change in alteration products. The lowest few meters of shale generally show strong argillic alteration. However the intensity of argillic alteration decreases upward in the section while the amount of pyrite and sericite present in the sedimentary rocks rapidly increases. The greater amount of pyrite deposited in the sedimentary rocks appears to be related to an increased carbonate content or porosity of a particular bed. Coincident with this change, some silicification of the most carbonate-rich beds occurs (although no jasperoid has yet been found in this unit). None of this alteration appears to be zoned around veins.

The flow and agglomerate member of the Copperopolis Latite that overlies the pyrite-rich lower member of the Golden's Ranch Formation typically exhibits alteration products indicative of less acidic conditions. The characteristic light green color of this unit (when altered) is imparted by abundant chlorite, which replaces matrix and phenocryst constituents, and contrasts with the kaolinite-dominant assemblage of the underlying tuff member (Kim, 1988). The flows which clearly vented from Sunrise Peak almost always exhibit this type of propyllitic (or chloritic) alteration. This difference, in the dominant alteration products, is probably not due to original differences in composition of these latitic units, inasmuch as these associations have been noted to be reversed in some outcrops of these units. Another common alteration characteristic of the agglomerate member is that quartz (clear euhedra) and calcite often line vugs and cavities while sparse limonite (after pyrite) occurs along fractures or small veinlets.

The alteration present in the upper lacustrine unit is more variable in intensity than the alteration present in underlying units. The shaley part of this unit is rarely exposed; however, one outcrop reveals that the basal part (~0.5 m) of the black, organic-rich shale contains abundant limonite, whereas the shale immediately above remains fresh and black. The lateral transition from limestone to jasperoid is also often abrupt (although recrystallization of the limestone may be more widespread). The most common variety of jasperoid found in this horizon is dense and black; however, various colors and porosities of jasperoid exist as well as variable amounts of interspersed limonite. Reflected light microscopy of vuggy, limonite-rich jasperoid reveals the presence of pyritohedral pyrite. Limestone adjacent to jasperoid generally exhibits evidence of substantial dissolution. The lateral variations in the alteration of this unit are probably related to proximity to hydrothermal conduits such as veins, faults, or dike margins.

Wide, persistent fissure veins generally occur in the more brittle or reactive rock types (such as the Paleozoic rocks and Tertiary porphyry intrusions). Consequently, significant veins have not been found in tuff, agglomerate, or lacustrine rock types, However, one small vein (15 cm wide) occurs in an agglomerate unit near Jumpoff Spring (Keith et al., 1989b) and exhibits a mineralogy consisting of quartz-calcite-dolomite-Fe-Mn-carbonates-barite-pyrite. With the exception of the carbonates, these gangue minerals are generally typical for many of the Tintic fissure veins. Other fragments of weathered vein material (also from veins approximately 10-15 cm wide with variable proportions of quartz and carbonates) occur as float in the general vicinity of Jumpoff Spring, but soil cover prohibits determination of their exact location. No veins of this width have been found that cut the lacustrine units.

### Mineral Compositions

The compositions of the individual mineral phases in the biotite latites flows and dikes and the Silver City Monzonite are unremarkable by themselves, but are generally equivalent; this reinforces the comagmatic interpretation of these units as indicated by the field and age relations and modal compositions. For example, the compositions of the clinopyroxenes in the flows, dikes, and monzonite of Silver City lithology are identical (Figure 6; Keith et al., 1989b). Although only a few analyses for plagioclase are available, the same correspondence is apparent (Keith et al., 1989b).

The compositions of the amphiboles from two widely seperated intrusions of Silver City Monzonite are also compared. One intrusion is adjacent to the concealed Cu-Mo deposit on the western side of the mapped area (Figure 1). The sample analyzed (TJ-164) has been intensely altered to the point that the stable mineral assemblage consists of epidote and amphibole. Amphibole from a comparatively fresh intrusion (TJ-153) exhibits an identical composition (Keith et al., 1989b).

According to the classification scheme of Leake (1978), this composition is magnesio-hastingsite - a term chosen to point out the comparatively Mg-rich composition. By comparison, the biotite present in the latite flows is relatively Mg- or phlogopite-rich (59-65 mole % phlogopite) as might be expected (Keith et al., 1989b). This accounts for the reciprocal occurrence of biotite and amphibole versus orthopyroxene (and sanidine) in the lavas (as also noted by Lindgren and Laughlin, 1919). Mg in the magma is incorporated in one of these three phases depending on the T, $fO_2$, $fH_2O$, and composition of the magma.

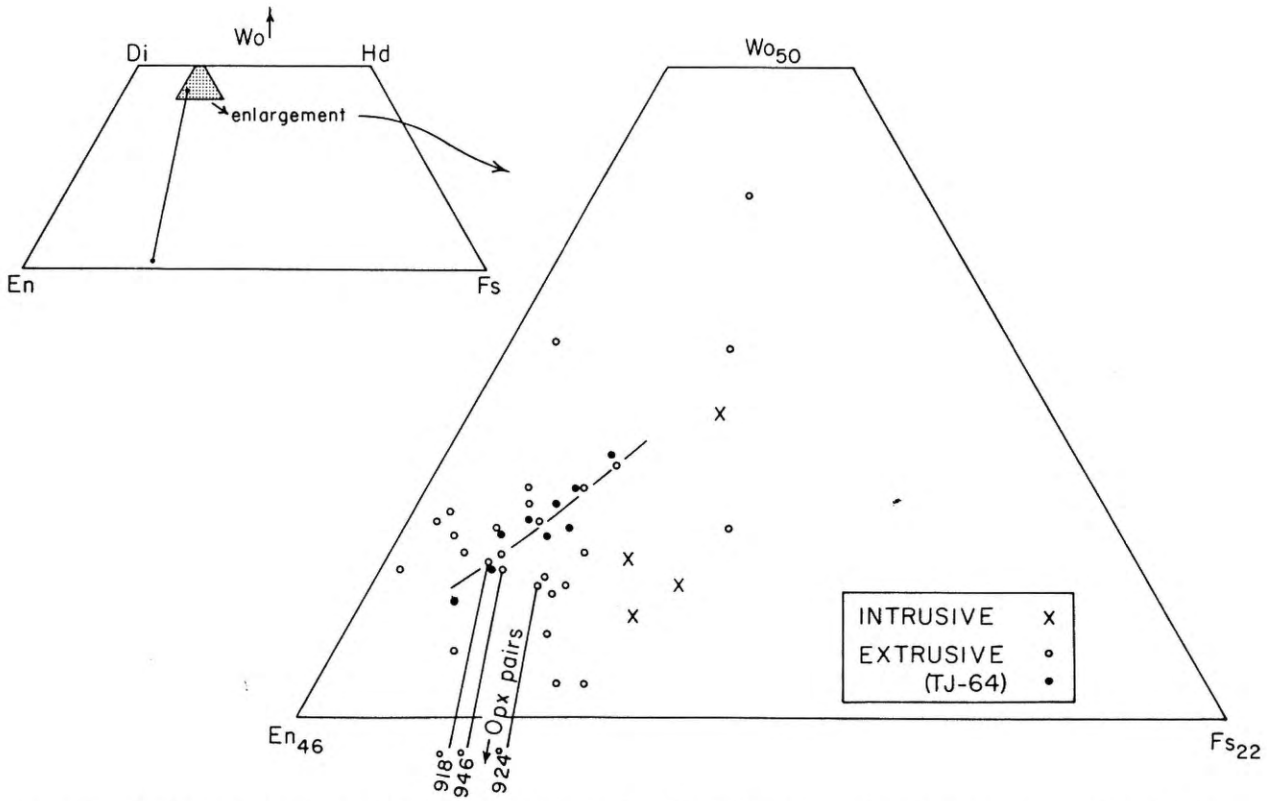


Fig. 6. Microprobe analyses of clinopyroxenes. Analyses from Table 3 are plotted on the pyroxene quadrilateral. Those clinopyroxenes with orthopyroxene pairs show the two pyroxene temperature for that pair along the tie-line (thermometer of Wells, 1977; compositions recalculated according to the methods of Lindsley and Anderson, 1983). Solid circles and best-fit line through them shows the compositional variations and trend present in one sample (TJ-64).

## Discussion

### Magmatic Sulfides

Immiscible magmatic sulfide blebs in intermediate to silicic magmas are probably quite common prior to eruption, but are generally either overlooked in chilled vitrophyres or they are removed during degassing of more slowly cooled lavas, tuffs, or intrusions. Hildreth (1977) noted magmatic pyrrhotite 1-10 microns in diameter sequestered within silicate and oxide phases from the Bishop Tuff. Whitney and Stormer (1983) and Drexler (1982) found pyrrhotite blebs of about the same dimensions within phenocrysts of the Fish Canyon Tuff and volcanic rocks of the Julcani district, Peru, respectively. The magmatic pyrrhotite which occurs in the rhyolite of Keystone Springs is similar in size and abundance to these pyrrhotite-bearing systems. However, the latites from the East Tintic Mountains contain magmatic sulfides which are both larger and more abundant by one to two orders of magnitude. This difference in size and abundance may be related to the fact that the East Tintic latites are more mafic than any of the previously mentioned calc-alkaline systems.

Magmatic sulfides from the East Tintic Mountains exhibit numerous similarities in mineralogy, morphology, and exsolution to those found in submarine basalts. Mathez (1976) surveyed the magmatic sulfide content of submarine basalt glasses from many localites; he found that magmatic sulfides were present in every glass examined. The most sulfide rich sample contained sulfide globules up to 100 microns in diameter with a total modal sulfide abundance of about 0.01%. Others have reported magmatic sulfides in basalts which range in volume up to 0.05% and in size up to 500 microns. The mineralogy of the Tintic sulfides is analogous to that of basalts. However, it appears that the parental MSS blebs from which the Tintic blebs were quenched were more sulfur rich than those calculated for most basalts. Tintic sulfides exsolved to form Ni-bearing pyrite rather than pentlandite. Tintic sulfides would clearly plot on the S-rich side of the MSS field on a Ni-Fe-S ternary diagram. Additionally, magnetite is not exsolved within the blebs as is often the case with more mafic compositions.

Tintic magmatic sulfides differ compositional from basaltic sulfides in two additional respects. The average Cu/Ni ratio for the Tintic magmatic sulfides (~15) is much higher than those reported for basalts (~2.0; Mathez, 1976) and similar estimates for Sudbury (~0.7 - 1.0; Naldrett, 1984). In addition, the average As content of the Tintic sulfides (~0.4%; Figure 4) is probably high inasmuch as As is generally unreported in analyses from other magmatic sulfides.

The relatively Ni-poor chracter of the Tintic magmatic

sulfides may be an indication that sulfides have been fractionated from the parental magmas during petrogenesis. Sulfide blebs (similar to the Tintic blebs) are common in xenoliths from the lower crust and upper mantle (Dromgoole and Pasteris, 1987). Lherzolites, which probably represent residuum of partial melting in the upper mantle, typically have Ni-rich (12 to 27 wt. %) sulfide blebs. Xenoliths derived from the lower crust have Ni-poor (<2 wt. %) blebs (Dromgoole and Pasteris, 1987). These data indicate that any residual sulfides left in the mantle during partial melting would tend to be Ni-rich relative to the portion of sulfide incorporated in the melt. In an similar fashion, the Ni-poor character and high Cu/Ni ratio of the Tintic blebs might indicate that more Ni-rich blebs may have been fractionated at some point between the mantle and the upper crust. If such an event happened those elements which have extremely high partition coefficients for immiscible sulfide melts (i.e. platinum group elements and Au) might also exhibit very low abundances in the Tintic magmas.

The most sulfide-rich samples of the Tintic latites may have been able to scavenge and concentrate any PGE or Au present in the melt. However, such sulfide-rich samples show no evidence of Pt, Pd, or Au concentrations above background values (5, 5, 1 ppb respectively). If the metal ratios of the magmatic blebs are partially inherited by the hydrothermal ores, then this may be one reason that the average Ag/Au ratio of the Tintic Districts is >100.

Some may be tempted to speculate that the seemingly fortuitous presence of large, abundant Cu-As-rich magmatic sulfides in the East Tintic volcanic rocks may be the result of upper crustal assimilation of mineralized rock. There is no evidence to indicate that upper crustal assimilation of a porphyry Cu-type deposit could account for the magmatic sulfides which occur as included blebs within every phenocrystic phase. Virtually every East Tintic volcanic unit for which fresh vitrophyres can be found contains at least a trace of magmatic sulfides. This thick volcanic sequence covers hundreds of square kilometers. In addition, magmatic pyrrhotite has also been found in a contemporaneous ash flow dike (35 Ma) which vented 30 km to the east of the East Tintic Mountains (Kim, 1988). Clearly, the magmatic sulfides are not the *result* of local assimilation of mineralized rock; however, they may have been degassed, dissolved, or resorbed after pluton emplacement to *contribute* to the hydrothermal ores. If so, their Cu-As-rich magmatic signature may be at least partially inherited by the hydrothermal ores.

Whitney (1984a, 1984b, 1988) and Whitney and Stormer (1983) have reviewed the potential role of pyrrhotite-bearing silicic magmas in providing a sulfur-bearing hydrothermal fluid for mineralization. The presence of pyrrhotite was used to estimate the fugacities of sulfurous gases in the parent magma chamber. The role of magmatic sulfide blebs in sequestering metals (i.e. Cu) during crystallization of the magma and releasing the metals after emplacement of an intrusion has been modeled by Candela (in press), but not critically evaluated using a pyrrhotite-bearing ore-related system. The Tintic magmatic sulfides provide an excellent opportunity to do so considering their unusually large size, abundance, and spatial and temporal relationship to productive plutons.

### Sulfur-Rich Magmas

A critical question that needs further study is why some units in a volcanic sequence are more sulfide-rich than others. For example, some Tintic biotite latites are clearly abnormally enriched in magmatic sulfides. High sulfur content may in part be inherited from subduction and partial melting of sulfide-rich oceanic crust (Whitney and Stormer, 1983). Alternatively, magma mixing may cause perturbations in S and O fugacities or FeO content sufficient to nucleate magmatic sulfides which are then concentrated by crystal settling (Figure 7; as suggested by many authors for sulfide-rich zones in layered intrusions). In addition, the solubility of S in a mafic (FeO-rich) melt is much greater than in a more silicic melt; consequently, a magma mixing scheme whereby sulfide saturated mafic magma (such as the mafic flows described in this report) mixes with more differentiated magma may create an unusually high amount of magmatic sulfides. Such mixing may be accompanied by a net decrease in confining pressure and $fO_2$ for the mafic constituent, which might then lower the solubility of S in the melt and increase the proportion of immiscible sulfide (Figure 7). This possibility is supported by the data of Carroll and Rutherford (1985) who have shown that sulfur solubility decreases with decreasing pressure and decreasing $fO_2$.

A third possibility is the introduction of crustal sulfur into the magma chamber by means of assimilation of sulfur-rich crustal rocks. Naldrett (in press) suggests that this process is critical to the formation of abundant magmatic sulfides in virtually all Cu-Ni deposits hosted by mafic intrusions with up to 75% of the sulfur being derived from assimilation of sulfate-rich (evaporites) country rocks. In terms of sulfur-rich volcanic rocks, Luhr et al. (1982) originally proposed a similar origin for the high sulfur content of the El Chichon volcanic rocks.

Some evidence from inclusions in the East Tintic latites suggests that assimilation of evaporites may have played a role in the formation of abundant magmatic sulfides. Our preliminary work found that one inclusion (which exhibits weak relict layering ?) which is present in a latite flow with abundant magmatic sulfides consists dominantly of hercynite and potassium feldspar and very minor sulfide blebs. The presence of hercynite precludes a magmatic origin for the inclusion; however it may represent a metamorphosed fragment of the gypsiferous Arapien Shale which may underlie both the volcanic complex and subjacent thrust sheets in this area (and may be almost 1 km thick) and form part of the country rock around the parent magma chamber. [Twenty

kilometers to the southest, where the Arapien Shale was encountered during drilling for oil it exhibits numerous beds of salt and gypsum up to 30 m thick.]

The isotopic signature of sulfides derived from sulfates would be very distinct from those formed by juvenile sulfur. Prior work on the S isotopic signatures of Tintic ores suggest values near -1.4 permil (Ames, 1970). Consequently, assimilation of evaporites would not appear to be an important contributor to the magmatic sulfides and subsequent hydrothermal ores. However, even minor assimilation of gypsiferous wallrocks may have kept the magma chamber near sulfide saturation over protracted episodes of fractionation and magma mixing. A sulfur isotope investigation of Tintic magmatic sulfides would help evaluate sources of sulfur and the potential buffering influence of evaporites to maintain sulfide saturation.

### Sulfide Exsolution and Degassing Processes

Sulfide blebs both in the lavas and the dikes exhibit various degrees of "replacement" by Fe oxide. This replacement is apparently related to the pressure decrease associated with eruption and the concurrent loss of sulfurous gases from the melt. In response sulfurous gases are also lost from the blebs leaving behind an Fe oxide residue. The process is important because, when such magma degasses at shallow levels in the crust, it may constitute the *birth* of the magmatic component of an ore fluid.

Some of the mineralogy and textures exhibited by the blebs can simply be attributed to quenching the bleb from magmatic temperatures without any loss of S or metals. Textural evidence suggests that the ISS (Cu-Fe-S) portion of the bleb is the first component to exsolve followed by the more Ni-rich (0.9-0.4% Ni) pyrite (Figure 7). In a closed system, approximated by a host crystal without cracks to the surface, the final assemblage is pyrrhotite, pyrite, chalcopyrite, and minor cubanite.

Magmatic sulfide blebs which are not tightly sequestered by phenocrysts exhibit an interesting mineralogical sequence of degassing. Examination of hundreds of blebs which exhibit various degrees of degassing from essentially none to complete suggests that some of the constituent sulfides are more stable than others. The first stage of this process appears to be pyrrhotite degassing to form a ferric oxide residue, As-rich pyrite, and sulfurous gas (Figure 7). The intergrowth of ferric oxide and the As-rich pyrite is controlled mainly by fractures in lava-hosted sulfides; dike-hosted magmatic sulfides exhibit a clear planar intergrowth of Fe oxide and As-rich pyrite (Figure 3) which is interpreted to be degassing along the basal cleavage of hexagonal pyrrhotite.

Whitney (1984b, 1988) demonstrates that the initial sulfurous gas evolved from strongly oxidized calc-alkaline magmas would be dominated by $SO_2$. He points out that the loss of this oxidized component would lower the $fO_2$ of the system to more reducing values; subsequently, $H_2S$ may exhibit the higher fugacity in the sulfurous gas. Whether or not the initial sulfurous gas emitted from the Tintic *sulfides* was dominated by $H_2S$ or $SO_2$ is unclear (Figure 7). The composition of titanomagnetites in the latites combined with two-pyroxene geothermometry (Figure 6) suggests that the conditions present in the parent magma chamber were near the $fSO_2 = fH_2S$ boundary. The lower solubility of $SO_2$ in the melt would indicate that initial gas lost after emplacement would be $SO_2$-dominated. It is important to note that the chalcopyrite portion of the bleb shows no evidence of degassing at this stage.

Fig. 7. Possible correlations between: A) magmatic proceses, B) magmatic sulfide bleb evolution, and C) Lindgren's (1949) sequential alteration stages. I. After formation of a caldera during eruption of the Copperopolis Tuff, subsequent volcanism within the caldera was dominantly intermediate (58-62 wt. % $SiO_2$) in composition with lesser amounts of more silicic and more mafic magma. Reductions in T, $fO_2$, P, and FeO content of mafic magma during magma mixing may have contributed to sulfide saturation and development of unusually large sulfide blebs. The high Cu content of the blebs may have allowed them to remain liquid at magmatic temperatures. II. Temporary waning of the influx of new magma may have allowed crystallization and crystal settling to develop a sulfide-rich magma at the base of the magma chamber. Large sulfide blebs were incorporated with glomeroporphyritic clots at the base or margins of the chamber. The ISS portion of the blebs began exsolving after the blebs had solidified, but exsolution was not complete until well after eruption or crystallization of the magma. III. A new cycle of eruption and intrusion created some flows which were poor in sulfides and others which were sulfide-rich. Sulfide blebs which were quenched in flows and shallow dikes, but were prevented from degassing consist dominantly of pyrrhotite (PYRR) with lesser Ni-Co-bearing pyrite (PY) and chalcopyrite (CHAL) $\pm$ cubanite (CUB). IV. The high $fO_2$ of the Tintic intermediate magmas combined with the low solubility of the $SO_2$ component of the magmatic sulfurous gases dictates that the initial magmatic volatiles lost from shallow intrusions will be $SO_2$-rich. Such emanations were likely responsible for creating the mid-barren stage of alteration. Magmatic sulfide blebs may have contributed some S at this stage ($SO_2$ if sufficient $O_2$ were present), but there is no indication that the blebs were resorbed or degassed quickly enough to supply metals to the exiting magmatic volatiles. V. After the loss of the $SO_2$-dominated sulfurous gases, the entire magmatic system as well as the sulfurous gases might be more reduced. The barren pyritic alteration of the late barren stage is an indication that the subsequent magmatic emanations were $H_2S$-dominated as would be anticipated. Magmatic sulfide blebs which were present in shallow dikes show strong evidence that the sulfurous gas exiting the blebs was reduced ($H_2S$) and created As-rich pyrite mantles on adjacent Fe silicate phenocrysts. The chalcopyrite remained undegassed at this stage. VI. Shallow dikes which exhibit a holocrystalline matrix, contain sulfide blebs which have completely degassed and have also partially or completely dissolved. This process was clearly capable of delivering Cu, Ag, Fe, As, and S to a hydrothermal fluid. In less quickly cooled magma, the sulfide blebs may have resorbed in response to the loss of sulfurous gases which were being exsolved from the melt and leaving the system. This final stage of bleb degassing, resorption, and solution could have provided some of the metals and help set metal ratios for the episode of mineralization.

## A. Magmatic Processes

I. Magma Mixing/Assimilation

II. Crystallization/Crystal Settling

III. Eruption/Intrusion

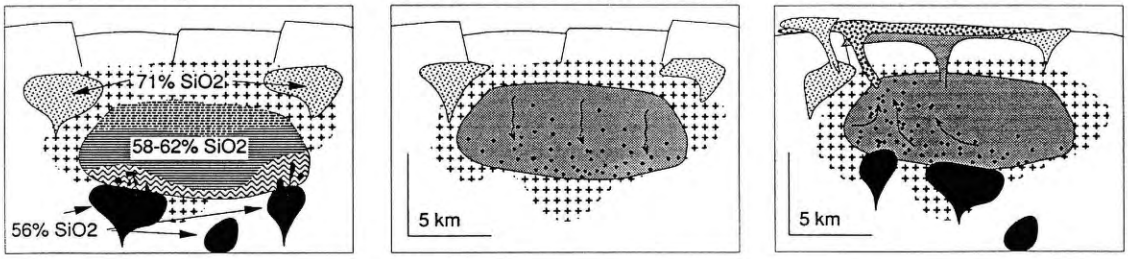


## B. Magmatic Sulfide Bleb Evolution

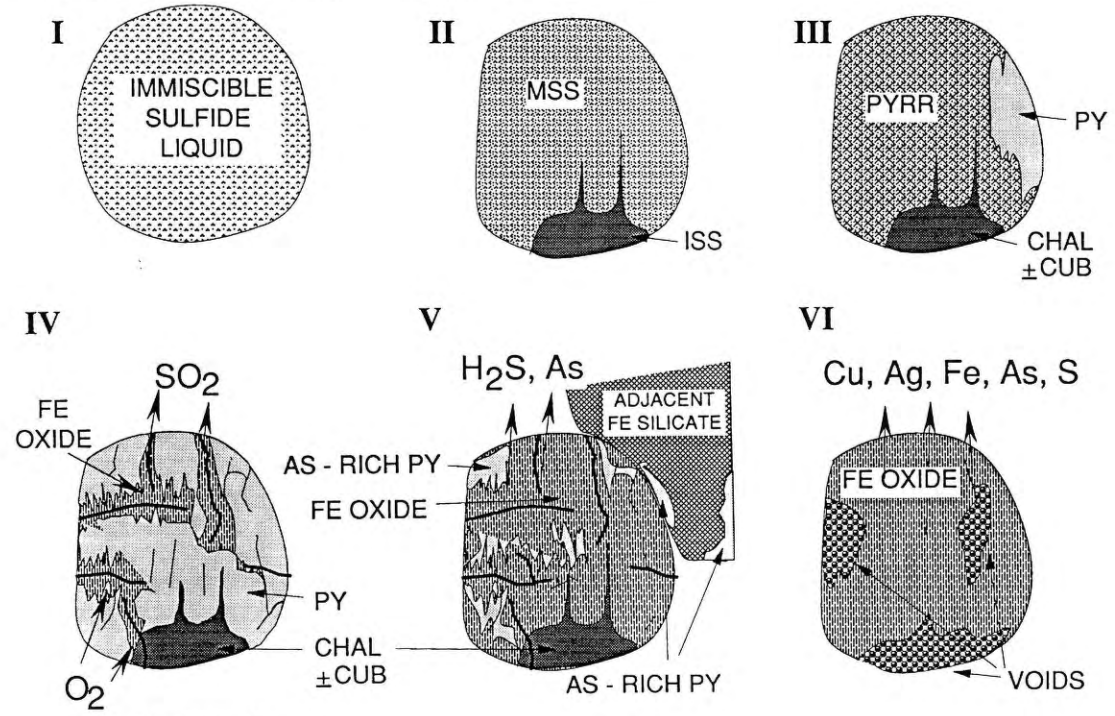


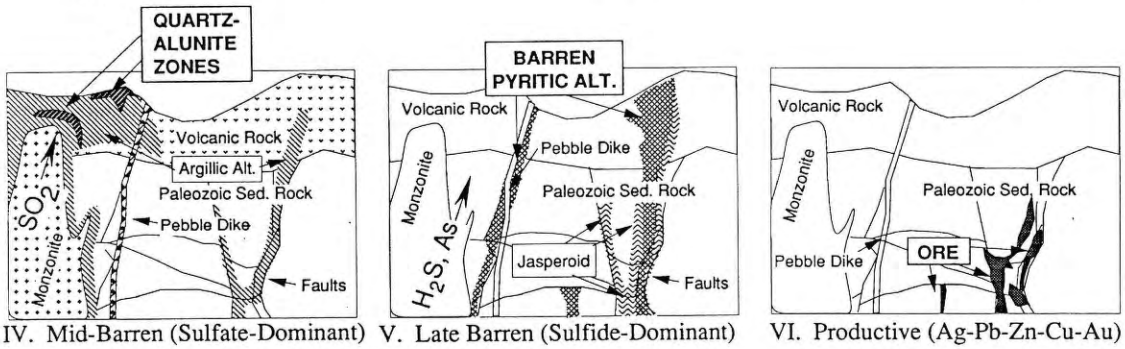


IV. Mid-Barren (Sulfate-Dominant) V. Late Barren (Sulfide-Dominant) VI. Productive (Ag-Pb-Zn-Cu-Au)

## C. Lindgren's (1949) Sequential Alteration Stages

The next mineral which is removed from the bleb is As-poor pyrite in favor of As-rich pyrite. Commonly the As-rich pyrite replaces adjacent biotite or clinopyroxene (Figure 3E and 3F) or reequilibrates within the bleb. This type of "sulfidation" is clearly due to removal of reduced S species from the bleb and reaction with reduced Fe in the silicates (Figure 7). For example, as the S escapes from blebs sequestered within biotite, it will sulfidize the cleavage trace it passes along and the S will be spent before the margin of the biotite crystal is reached. Arsenic appears to be a key factor in temporarily stabilizing pyrite during bleb degassing. The result is prong of As-rich pyrite extending outward from the bleb (Figure 3E). The replaced margins of pyroxene remain perfectly euhedral (Figure 3F). This process is a strong indication that $H_2S$ is the dominant sulfur species in the system as might be indicated by the data of Whitney (1988). $H_2S$ (and As?) would also be important constituents in any magmatic vapor leaving the system. Whether or not this stage of bleb degassing is mediated by magmatic water vapor or hydrothermal fluid is unclear. The matrix of such samples varies from perlitic to microcrystalline. However, any reaction that can be written that produces ferric iron within the bleb and $H_2S$ as the degassed component, would consume substantial water. One possibility would include: $H_2 + 4H_2O + 2FeS_2 = 4H_2S + Fe_2O_3 + H_2O$. Such a reaction might account for the persistence of ferric iron within the bleb adjacent to unaffected As-rich pyrite and magnetite. However, even at this stage of degassing, the chalcopyrite portion of the bleb remains dominantly intact (Figure 7).

The final stage of bleb degassing is characterized by complete removal of sulfides from the bleb as well as part or all of the residual Fe (Figure 7). The matrix of such samples is completely crystalline. The process likely involves solution of the bleb more than degassing. Residual Fe in the blebs still contains substantial Ni and Co (Figure 4). The residual Fe in the bleb is preferentially dissolved by the hydrothermal fluid while adjacent magnetite is unaffected. Cu, As, Fe, (Ag?), and S are clearly mobilized by the hydrothermal fluid and presumably could be transported out of the intrusion.

If these elements are being completely removed from the dikes and lavas in response to these degassing processes, then whole-rock analyses may illustrate the loss. In this regard, Cu and As abundances do show some correlation (Figure 5). Petrograhic examination of the samples illustrated in Figure 5 reveals that the most As-rich samples contain abundant magmatic sulfides. The most As-poor samples are represented by latite vitrophyres which contain abundant magmatic sulfides which have completely degassed to Fe-oxide or they represent sulfide-absent monzonite porphyry. The points joined by a tie-line represent a sulfide-rich latite vitrophyre (on the left) and a panned heavy mineral concentrate of the same sample. The sharp increase in Ag and Cu which occurs with an increase in As-bearing sulfides is *permissive* evidence that the Cu *and Ag* are both hosted largely by the sulfides. This is petrographically obvious for the Cu, but is inferred for the Ag. Alternatively, the Ag could be dominantly present in the clinopyroxene and titanomagnetite in the concentrate, but this seems less likely. It is interesting to note that the Au content of both the sample and the concentrate are at the detection limit of 1 ppb.

The stages of bleb degassing outlined here are derived from examination of fresh, quickly chilled, high level dikes and lava vitrophyres. These processes may not be an accurate guide to the fate of magmatic sulfide blebs throughout the dominant volumes of the intrusions. If the magma is not as quickly chilled, the sulfide blebs may simply be resorbed as the melt-hosted sulfurous gases exit the magma or intrusion. Sulfide blebs hosted entirely by glass or perlite do often show evidence of the initiation resorption prior to quenching (Figure 3D). In any case, the melt-hosted sulfurous gases may leave the magma first; the metals, S, and As sequestered by the blebs would lag behind whether they are removed by degassing, resorption, or solution.

Examination of the *sequential* hydrothermal alteration stages (Lovering, 1949) in the Tintic mining districts suggests that such a decoupling of S and metals may have occurred. The U.S. Geological Survey spent many years examining the hydrothermal alteration patterns of the Tintic mining districts; the studies surmized that the alteration zones present in the districts were the result of "*different solutions* which followed the same paths at *different times*" (Lovering, 1949). The first alteration stages were notably barren of any trace of mineralization. The enormous volume of intensely altered (pyrite-bearing) volcanic rocks in the East Tintic Mountains which is totally barren of mineralization to a large degree sets these districts apart from many other mining districts in the Great Basin.

The first alteration stage which is spatially related to the monzonite intrusions is the "mid-barren" stage which could generally be descibed as argillic. The hydrothermal solutions were interpreted to be sulfate-dominated and produced alunite spatially zoned around the parental intrusion at shallow depths (Figure 7). This stage of alteration could have easily been produced from the initial rapid loss of $SO_2$ from the magma which might accompany injection of the magma into vents or shallow intrusions. Considering the proportion of sulfide blebs trapped by phenocrysts and glomeroporphyritic clots, the metals hosted by the blebs may have been sequestered from this initial sulfate degassing episode.

The subsequent alteration stage is also notably barren and is called the "late-barren" stage. The spatial relationship of this stage to monzonite intrusions is not as close as the previous stage (Figure 7). Lovering (1949) describes the causitive hydrothermal fluid as "gas-phase hydrogen sulfide" which converts Fe silicates and magnetite in the lavas to pyrite. After loss of the weakly soluble $SO_2$ during the mid-barren stage, the remaining magma and sulfurous gases could easily have been driven into the T-$fO_2$ region where $H_2S$ is the dominant sulfurous gas (Whitney, 1984b, 1988). Continued degas-

sing of the melt-hosted sulfurous gases in the magma could have produced the barren pyritic portion of this alteration stage (Figure 7). Initial degassing of the blebs may have contributed some $H_2S$ as well.

The Tintic districts also commonly exhibit abundant As anomalies which show no close relationship to mineralization in time or space. The pyrite-rich alteration present in the Tertiary lacustrine sedimentary rocks exhibits As anomalies of at least a few hundred ppm. The sample of a small vein from Government Canyon described previously contains 4800 ppm As, but no anomalous metals. Clearly, the initial sulfurous gases released from the Tintic monzonitic magmas may have been accompanied by As, but not metals. The bleb degassing sequence noted in the latites (Figure 7) strongly indicates that $H_2S$ and As removal may largely precede removal of magmatic chalcopyrite (and any chalcopyrite-hosted precious metals).

A one-to-one correspondence of magmatic sulfide composition and metal ratios in the Tintic hydrothermal ores is not proposed. However, these data certainly indicate that magmatic sulfides are capable of sequestering and then giving a delayed release to important chalcophile constituents of hydrothermal ores. Other ore-related systems which are not sulfide saturated or have fewer and smaller magmatic sulfides may not show a "decoupling" of barren alteration and mineralization as in the Tintic districts.

The salinity and composition of the hydrothermal fluid are undoubtedly important in determining the metal ratios of a deposit. For example, important constituents of the Tintic ores (Pb, Zn, Ba) might be leached from the silicate and oxide minerals of the monzonite depending on the temperature and composition of the fluid. However, the *availability* of metals, whether those metals are present in melt, oxide, silicate, or sulfide phases would help determine the *metal ratios* of the deposit (i.e. Ag/Au) and the *grade*. Whether the parental magma of an ore deposit is merely sulfide-saturated or has become enriched in magmatic sulfides by one to two orders of magnitude would certainly have an effect on the grade of the resultant deposit. Layered mafic and ultramafic intrusions clearly show that crystal fractionation (often preceded by magma mixing) is capable of creating substantial enrichments of magmatic sulfides and contained Cu, Ni, and PGE. The wide variations in the magmatic sulfide content of the latites from the East Tintic Mountains suggests that sulfide-rich magmas ultimately may be partly responsible for creating the large volume of high-grade ore in these districts.

The coincidence in age between the sulfide-rich latite (34.5 Ma) and the adjacent porphyry Cu-Mo prospect (34.4 Ma; Hannah and Macbeth, 1990) suggests that the parental magma of the porphyry Cu-Mo deposit was almost certainly comagmatic with the sulfide-rich latitic magma. Resorption of magmatic sulfide blebs may have provided an important flux of Cu-rich volatiles to the porphyry Cu-Mo stock.

Some of the volcanic and intrusive units from the East Tintic Mountains are the same age and/or composition as the main intrusive units of the Bingham porphyry Cu deposit (65 km to the north). Lindgren and Loughlin (1919) were impressed with similarities between the mineralization and ore-related porphyries of these two systems to the point that they proposed that they were fed from the same parental magma chamber. It is very unlikely that the two are comagmatic. However, the discovery of Cu-bearing magmatic sulfides in volcanic units from the East Tintic Mountains may have important implications concerning the genesis of the porphyry Cu deposits, such as Bingham, as well. It was Lindgren and Loughlin (1919) who first confidently proposed that the monzonite dikes and intrusions are the ultimate source of the base- and precious-metals which form the deposits in these districts. However, the discovery of unusually large and abundant Cu-As-(Ag-)bearing magmatic sulfides in ore-related dikes may be important evidence for their model. The degassing and resorption of these magmatic sulfides, which occurs after depressurization of the magma, may represent the *birth* of an important component of the ore fluid.

## Conclusions and Summary

This report documents several new findings concerning the geology and mineralogy of volcanic units in the central East Tintic Mountains, Utah. For example, fission-track ages and $^{40}Ar/^{39}Ar$ ages which we report suggest that some of the volcanism in this area which is contemporaneous or stratigraphically beneath the lacustrine horizons is as old as ca. 37.4 to 35.3 Ma (Figure 2). Age determinations for units above the lacustrine horizons (or for intrusions which cut them) range from 34.5 to 33.6 Ma. This implies that a large caldera related to the eruption of the younger Packard Quartz Latite and Fernow Quartz Latite is not present in this area. However, our data suggests that a smaller caldera related to the eruption of the tuff member of the Copperopolis Latite may be present. We note that many monzonite dikes and intrusions in this area are hornblende bearing and are correlative in modal and chemical composition with the productive Silver City Stock rather than the barren Sunrise Peak Stock. The large areas of hydrothermal alteration which surround these intrusions exhibit many similarities to the well-studied alteration halos in the East Tintic District. The age, composition, and field relationships of the post-lacustrine volcanic rocks suggest that they may represent, in part, the extrusive equivalents of the monzonite dikes and Silver City Stock. Our work suggests that the Silver City Stock and related intrusions may be part of one of the youngest ($33.6 \pm 0.2$ Ma) igneous events in the central East Tintic Mountains, but not as young as previously suggested (ca. 31.5 Ma).

In addition, our recent work has documented the existence of unusually large (and abundant) *magmatic* sulfides in lava vitrophyres and vent-facies biotite latite

dikes, which are the surface expressions of the Silver City Quartz Monzonite intrusions in this area. The abundance and diameters of sulfide blebs between various units varies widely. The most sulfide-rich biotite latite glass from the East Tintic Mountains which has been found so far contains globules up to 450 microns in diameter with a modal abundance of 0.02% (Figure 3). Careful modal analysis of the sulfide distribution in one sample revealed a total of 465 sulfide blebs over 1 micron in size in one thin section. Titanomagnetite contained 36% of the blebs, clinopyroxene contained 27%, the matrix 22%, biotite 10%, and plagioclase contained only 4%.

By comparison, several vitrophyres are relatively sulfide-poor. Standard petrographic thin sections of such vitrophyres commonly contain fewer than 10 sulfide blebs with diameters in the range of 1-10 microns.

Some of the mineralogy and textures exhibited by the blebs can simply be attributed to quenching the bleb from magmatic temperatures without any loss of S or metals. Textural evidence suggests that the ISS (Cu-Fe-S) portion of the bleb is the first component to exsolve followed by the more Ni-rich (0.9-0.4% Ni) pyrite (Figure 7). In a closed system, approximated by a host crystal without cracks to the surface, the final assemblage is pyrrhotite, pyrite, chalcopyrite, and minor cubanite. In addition, preliminary analytical data suggest that the sulfides host most (~75%) of the Ag present in the latites.

The East Tintic Mountains are potentially the first locality, worldwide, where some of the metal in mesothermal veins can be demonstrated to be derived from degassed magmatic sulfides. In addition, the decoupling of barren alteration and mineralization in the East Tintic Mountains may be related to the observed sequence of sulfide bleb degassing, resorption and solution. For example, the high $fO_2$ of the Tintic intermediate magmas combined with the low solubility of the $SO_2$ component of the magmatic sulfurous gases dictates that the initial magmatic volatiles lost from shallow intrusions will be $SO_2$-rich. Such emanations were likely responsible for creating the sulfate-dominated mid-barren stage of alteration. Magmatic sulfide blebs may have contributed some S at this stage, but there is no indication that the blebs were resorbed or degassed quickly enough to supply metals to the exiting magmatic volatiles.

After the loss of the $SO_2$-dominated sulfurous gases, the entire magmatic system as well as the sulfurous gases might be more reduced. The barren pyritic alteration of the late barren stage is an indication that the subsequent magmatic emanations were $H_2S$-dominated as would be anticipated. Magmatic sulfide blebs which were present in shallow dikes show strong evidence that the sulfurous gas exiting the blebs was reduced ($H_2S$) and created As-rich pyrite mantles on adjacent Fe silicate phenocrysts. The chalcopyrite remained undegassed at this stage. Shallow dikes which exhibit a holocrystalline matrix, contain sulfide blebs which have completely degassed and have also partially or completely dissolved (Figure 7). This process was clearly capable of delivering Cu, Ag, Fe, As, and S to a hydrothermal fluid. In less quickly cooled magma, the sulfide blebs may have resorbed in response to the loss of sulfurous gases which were being exsolved from the melt and leaving the system. This final stage of bleb degassing, resorption, and solution could have provided some of the metals and help set metal ratios for the episode of mineralization.

A one-to-one correspondence of magmatic sulfide composition and metal ratios in the Tintic hydrothermal ores is not proposed. However, these data certainly indicate that magmatic sulfides are capable of sequestering and then giving a delayed release to important chalcophile constituents of hydrothermal ores. Other ore-related systems which are not sulfide saturated or have fewer and smaller magmatic sulfides may not show a decoupling of barren alteration and mineralization as in the Tintic districts.

## Acknowledges

This study was funded in part by contract # 88-3548 with the Utah Geological and Mineral Survey. Their assistance is gratefully acknowledged. Discussions and field excursions with Glenn Mellor, Judy Hannah, Grant Willis, Eric Christiansen, Mark Jensen, Mike Shubat, and Bob Gloin helped modify or formulate some of our ideas. The help of two anonymous reviewers is greatfully acknowledged. In addition, Judy Hannah kindly provided us with a biotite concentrate of the Silver City Stock which was used for $^{40}Ar/^{39}Ar$ age spectrum analysis.

## References

Alexander, E. C., Jr., Michelson, G. M., and Lanphere, M. A., 1978, MMhb-1: A new $^{40}Ar/^{39}Ar$ dating standard, *in* Zartman, R. E., ed., Short papers of the Fourth International Conference, Geochronology, Cosmochronology, Isotope Geology: U.S. Geological Survey Open-File Report 78-701, p. 6-8.

Candela, P. A., in press, Felsic magmas, volatiles, and metallogenesis: in Whitney, J. A., and Naldrett, A. J., eds., Ore deposition Associated with Magmas, Reviews in Economic Geology, v. 4.

Carroll, M. R., and Rutherford, M. J., 1985, Sulfide and sulfate saturation in hydrous silicate melts: Journal of Geophysical Research, v. 90, suppl. C601-C612.

Craig, J. R., and Scott, S. D., 1974, Sulfide phase equilibria: in Ribbe, P. H., ed., Sulfide Mineralogy, Mineralogical Society of America Short Course Notes, v. 1, p. CS-1 to CS-110.

Dalrymple, G. B., Alexander, E. C., Lanphere, M. A., and Kraker, G. P., 1981, Irradiation of samples for $^{40}Ar/^{39}Ar$ dating using the Geological Survey TRIGA reactor: U.S. Geological Survey Professional Paper 1176, 55 p.

Distler, V. V., Genkin, A. D., and Dyuzhikov, O. A., 1986, Sulfide petrology and genesis of copper-nickel ore deposits: in Friedrich, G. H., Genkin, A. D., Naldrett, A. J., Ridge, J. D., Sillitoe, R. H., and Vokes, F. M., eds., Geology and Metallogeny of Ore Deposits, p. 111-123.

Drexler, J. W., 1982, Mineralogy and geochemistry of Miocene volcanic rocks related to the Julcani Ag/Au/Cu/Bi deposit, Peru: Physiochemical conditions of a productive magma body: Unpub. Ph.D dissert., Houghton, Michigan Technological University, 250 p.

Dromgoole, E. L., and Pasteris, J. D., 1987, Interpretation of sulfide assemblages in a suite of xenoliths from Kilbourne Hole, New Mexico: Geological Society of America Special Paper 215, p. 25-46.

Gillerman, V. S., 1986, Barren hot spring alteration versus precious metal related alteration, Tintic district, Utah: Geological Society of America Abstracts with Programs, v. 18, p. 614.

Hannah, J. L., and Macbeth, A., 1990, Magmatic history of the East Tintic Mountains, Utah: U.S. Geological Survey Open-File Report 90-0095, 20 p.

Harrison, T. M. and Fitzgerald, J. D., 1986, Exsolution in hornblende and its consequences for $^{40}Ar/^{39}Ar$ age spectra and closure temperature: Geochimica et Cosmochimica Acta, v. 50, p. 247-253.

Hildreth, E. W., 1977, The magma chamber of the Bishop Tuff: Gradients in temperature, pressure, and composition: unpublished Ph.D. dissertation, University of California, Berkeley, 328 p.

Keith, J. D., Dallmeyer, R. D., and Kowallis, B. J., 1989a, Latite with magmatic pyrrhotite: A possible precursor to monzonite-related alteration/mineralization in the East Tintic Mountains, Utah: Geological Society of America Abstracts With Programs, v. 21, p. 100.

Keith, J. D., Dallmeyer, R. D., Kim, C. S., and Kowallis, B. J., 1989b, A re-evaluation of the volcanic history and mineral potential of the central East Tintic Mountains, Utah: Utah Geological and Mineral Survey Open-File Report 166, 74 p.

Kim, C. S., 1988, Geochemical aspects of Eocene-Oligocene volcanism and alteration in central Utah: unpub. M. S. thesis, University of Georgia, Athens, 106 p.

Kim, C. S., and Keith, J. D., 1989, Stratigraphically-controlled alteration related to sub-volcanic intrusions in the central East Tintic Mountains, Utah: Geological Society of America Abstracts With Programs, v. 21, p. 101.

LeVot, M., 1984, L'overthrust belt face aux Uinta Mountains, Utah [These de Doctorat]: Orleans, France, Universite D'Orleans, 278 p.

Lightfoot, P. C., Naldrett, A. J., and Hawkesworth, C. J., 1984, The geology and geochemistry of the Waterfall Gorge section of the Insizwa complex with particular reference to the origin of the nickel sulfide deposits: Economic Geology, v. 79, p. 1857-1879.

Lindgren, Waldemar, and Loughlin, G. F., 1919, Geology and ore deposits of the Tintic mining district, Utah: U.S. Geological Survey Professional Paper 107, 282 p.

Lovering, T. S., 1949, Rock alteration as a guide to ore - East Tintic district, Utah: Economic Geology Monograph 1, 65 p.

Luhr, J., Carmichael, I. S. E., and Varecamp, J. C., 1982, Eruption of El Chichon volcano, Chipas, Mexico: EOS (Transactions of the American Geophysical Union), v. 63, p. 1126-1127.

Mathez, E. A., 1976, Sulfur solubility and magmatic sulfides in submarine basalt glass: Journal of Geophysical Research, v. 81, p. 4269-4276.

Morris, H. T., 1975, Geologic map and sections of the Tintic Mountain quadrangle and adjacent part of the McIntyre quadrangle, Juab and Utah Counties, Utah: U.S. Geological Survey Map I-883.

Morris, H. T., and Lovering, T. S., 1979, General geology and mines of the East Tintic mining district, Utah and Juab Counties, Utah: U.S. Geol. Survey Professional Paper 1024, 203 p.

Morris, H. T., and Morgensen, A. P., 1978, Tintic Mining district, Utah: Brigham Young University Geology Studies, v. 25, p. 33-45.

Naldrett, A. J., in press, Sulfide melts: Crystallization temperatures, solubilities in silicate melts, and Fe-Ni-Cu partitioning between basaltic magmas and olivine: in Whitney, J. A., and Naldrett, A. J., eds., Ore deposition Associated with Magmas, Reviews in Economic Geology, v. 4.

Norrish, K., and Hutton, J. T., 1969, An accurate X-ray spectrographic method for the analysis of a wide range of geologic samples: Geochimica et Cosmochimica Acta, v. 33, p. 431-453.

Roddick, J. C., 1978, The application of isochron diagrams in $^{40}Ar/^{39}Ar$ dating: A discussion: Earth and Planetary Science Letters, v. 41, p. 233-244.

Steiger, R. H. and Jager, E., 1977, Subcommission on geochronology: Convention on the use of decay constants in geo- and cosmochronology: Earth and Planetary Sciences, v. 36, p. 359-362.

Villien, A., 1984, Central Utah deformation belt: unpub. Ph.D. thesis, University of Colorado, 282 p.

Wells, P. R. A., 1977, Pyroxene thermometry in simple and complex systems: Contributions to Mineralogy and Petrology, v. 62, p. 586-594.

Werle, J. L., Ikramuddin, M., and Mutschler, F. E., 1984, Allard stock, La Plata Mountains, Colorado—an alkaline rock-hosted porphyry Cu - precious metal deposit: Canadian Journal of Earth Science, v. 21, p. 630-641.

Whitney, J. A., 1984a, Fugacities of sulfurous gases in pyrrhotite-bearing silicic magmas: American Mineralogist, vol. 69, p. 69-78.

Whitney, J. A., 1984b, Volatiles in magmatic systems: Reviews in Economic Geology, v. 1, p. 154-175.

Whitney, J. A., 1988, Composition and activity of sulfurous species in quenched magmatic gases associated with pyrrhotite-bearing silicic systems: Economic Geology, v. 83, p. 86-92.

Whitney, J. A., and Stormer, J. C., Jr., 1983, Igneous sulfides in the Fish Canyon Tuff and the role of sulfur in calc-alkaline magmas: Geology, v. 11, p. 99-102.

Whitney, J. A., Hemley, J. J., Simon, F. O., 1985, The concentration of iron in chloride solutions equilibrated with synthetic granitic compositions: The sulfur free system: Economic Geology, v. 80, p. 444-460.

Willis, G. C., 1986, Geologic map of the Salina Quadrangle: Utah Geological and Mineral Survey Map 83.

Witkind I. J., and Marvin, R. F., 1989, Significance of new potassium-argon ages from the Goldens Ranch and Moroni Formations, Sanpete-Sevier Valley area, central Utah: Geological Society of America Bulletin, v. 101, p. 534-548.

York, D., 1969, Least squares fitting of a straight line with correlated errors: Earth and Planetary Science Letters, v. 5, p. 320-324.

# Geology and Ore Deposits of the Great Basin

## Symposium Proceedings

Editors: Gary L. Raines, Richard E. Lisle
Robert W. Schafer, and William H. Wilkinson

*Sponsored by the Geological Society of Nevada*
*and United States Geological Survey*
*April 1-5, 1990*

*Published by*
*Geological Society of Nevada*
*Reno, Nevada 1991*